Oceanic controls on the mass balance of Wilkins Ice Shelf, Antarctica

Laurie Padman,[1] Daniel P. Costa,[2] Michael S. Dinniman,[3] Helen A. Fricker,[4] Michael E. Goebel,[5] Luis A. Huckstadt,[6] Angelika Humbert,[7] Ian Joughin,[8] Jan T. M. Lenaerts,[9] Stefan R. M. Ligtenberg,[9] Ted Scambos,[10] and Michiel R. van den Broeke[9]

Received 16 May 2011; revised 21 October 2011; accepted 4 November 2011; published 20 January 2012.

[1] Several Antarctic Peninsula (AP) ice shelves have lost significant fractions of their volume over the past decades, coincident with rapid regional climate change. Wilkins Ice Shelf (WIS), on the western side of the AP, is the most recent, experiencing a sequence of large calving events in 2008 and 2009. We analyze the mass balance for WIS for the period 1992−2008 and find that the averaged rate of ice-shelf thinning was $\sim$0.8 m a^{-1}, driven by a mean basal melt rate of $\langle w_b \rangle$ = 1.3 $\pm$ 0.4 m a^{-1}. Interannual variability was large, associated with changes in both surface mass accumulation and $\langle w_b \rangle$. Basal melt rate declined significantly around 2000 from 1.8 $\pm$ 0.4 m a^{-1} for 1992–2000 to $\sim$0.75 $\pm$ 0.55 m a^{-1} for 2001–2008; the latter value corresponding to approximately steady-state ice-shelf mass. Observations of ocean temperature T obtained during 2007–2009 by instrumented seals reveal a cold, deep halo of Winter Water (WW; $T \approx -1.6$°C) surrounding WIS. The base of the WW in the halo is $\sim$170 m, approximately the mean ice draft for WIS. We hypothesize that the transition in $\langle w_b \rangle$ in 2000 was caused by a small perturbation ($\sim$10–20 m) in the relative depths of the ice base and the bottom of the WW layer in the halo. We conclude that basal melting of thin ice shelves like WIS is very sensitive to upper-ocean and coastal processes that act on shorter time and space scales than those affecting basal melting of thicker West Antarctic ice shelves such as George VI and Pine Island Glacier.

Citation: Padman, L., et al. (2012), Oceanic controls on the mass balance of Wilkins Ice Shelf, Antarctica, *J. Geophys. Res.*, *117*, C01010, doi:10.1029/2011JC007301.

1. Introduction

[2] Most of the ice shelves around the Antarctic Peninsula (AP) have retreated or collapsed during the last several decades [*Cook and Vaughan*, 2010], and the majority of marine-terminating glaciers have also retreated [*Cook et al.*, 2005]. The remaining large AP ice shelves that have relatively stable areal extents have experienced surface lowering [*Zwally et al.*, 2005; *Fricker and Padman*, 2012]. These ice mass losses have occurred during decades of changing regional climate including rising air temperature across the AP [*Vaughan and Doake*, 1996], rising deep water temperatures in the Weddell Sea [*Robertson et al.*, 2002], and rising ocean temperature [*Martinson et al.*, 2008] and reduced sea-ice coverage [*Stammerjohn et al.*, 2008] on the continental shelf on the western side of the AP. We assume that there is a causal connection between environmental changes and ice loss; however, the actual mechanisms are poorly understood, and we expect them to vary from one ice shelf to another.

[3] Wilkins Ice Shelf (WIS), located on the western side of Alexander Island, is the most recent AP ice shelf to undergo significant retreat. With a total area of $\sim$11,144 km^2 as of 2008/2009 [*Cook and Vaughan*, 2010], WIS is the fourth largest remaining ice shelf on the AP (Figure 1). The WIS lies landward of the broad continental shelf of the southern Bellingshausen Sea, hereafter denoted sBS.

[4] The WIS experienced four large breakup events in 2008 and 2009. An area of $\sim$425 km^2 disintegrated between

[1]Earth and Space Research, Corvallis, Oregon, USA.
[2]Ecology and Evolutionary Biology, University of California, Santa Cruz, California, USA.
[3]Center for Coastal Physical Oceanography, Old Dominion University, Norfolk, Virginia, USA.
[4]Institute of Geophysics and Planetary Physics, Scripps Institution of Oceanography, University of California, San Diego, La Jolla, California, USA.
[5]Antarctic Ecosystem Research Division, SWFSC, National Marine Fisheries Service, NOAA, La Jolla, California, USA.
[6]Ocean Sciences, University of California, Santa Cruz, California, USA.
[7]Institute of Geophysics, University of Hamburg, Hamburg, Germany.
[8]Polar Science Center, Applied Physics Laboratory, University of Washington, Seattle, Washington, USA.
[9]Institute for Marine and Atmospheric Research Utrecht, Utrecht University, Utrecht, Netherlands.
[10]National Snow and Ice Data Center, CIRES, University of Colorado at Boulder, Boulder, Colorado, USA.

0148-0227/12/2011JC007301

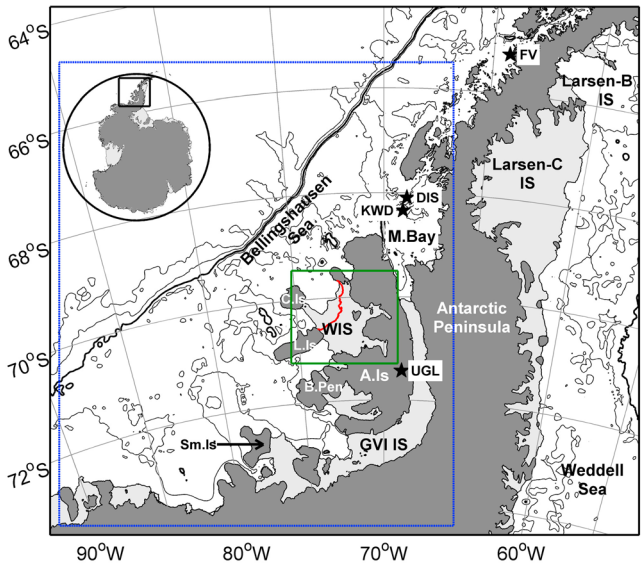

Figure 1. Map of Antarctic Peninsula showing locations described in text: WIS; GVIIS; Larsen B and Larsen C ice shelves; Alexander, Charcot, Latady, and Smyley islands (A.Is, C.Is, L.Is, Sm.Is); Beethoven Peninsula (B.Pen), Marguerite Bay (M.Bay); automatic weather stations (AWS) at Dismal Island (DIS), Kirkwood Island (KWD), and Uranus Glacier (UGL); and location of SSH record at Verdansky (formerly Faraday) Station (FV). WIS extent is based on the Mosaic of Antarctica [*Scambos et al.*, 2007], compiled from Moderate Resolution Imaging Spectroradiometer images from 2003/2004. Red line across northern WIS is the ice front in February 2011. Contours indicate 500, 1000, 2000, and 3000 m isobaths from the TOPO 11.1 bathymetry grid. The 1000 m contour is bold, to show the approximate outer limit of the continental shelf. Green rectangle indicates area covered by Figures 2 and 4. Blue dashed rectangle indicates area covered by Figures 6, 9, and 10.

28 February and 6 March 2008 [*Braun and Humbert*, 2009; *Scambos et al.*, 2009]. Another ~160 km^2 was lost in a smaller breakup event during 30–31 May 2008, followed by a further loss of ~1220 km^2 in austral winter (28 June to 15 July 2008) [*Humbert and Braun*, 2008]. In April 2009, a narrow "ice bridge" connecting Charcot and Latady islands (see Figure 2) finally failed [*Humbert et al.*, 2010], leading to an additional loss of ~730 km^2 as previously rifted areas along the northern ice front subsequently detached. As of March 2011, the total area lost (~2500 km^2) since the start of 2008 represents about 20% of the original area (~13,660 km^2), with an additional ~2370 km^2 of the remaining ice shelf now visibly rifted. Retention of some of the remaining intact ice shelf may be assisted by several small ice rises [*Braun et al.*, 2009].

[5] The total area lost from WIS during 2008 and 2009 is quite small compared with large iceberg calving events from other ice shelves; for example, ~11,000 km^2 for iceberg B-15 that calved from Ross Ice Shelf in March 2000 [*Lazzara et al.*, 1999]. However, larger, single-iceberg calving events are understood to be part of a recurrent cycle of ice-shelf advance and retreat [e.g., *Fricker et al.*, 2002], whereas collapse events represent shifts in ice-shelf state that appear to be driven by changes in climate.

[6] The preceding major ice-shelf collapse event along the AP, the rapid breakup of Larsen B Ice Shelf in 2002, is believed to have been caused by the action of meltwater forming on the ice-shelf surface in response to increased summer air temperatures following an extended period of atmospheric warming [*Scambos et al.*, 2003; *MacAyeal et al.*, 2003; *van den Broeke*, 2005]. A change in the internal ice-shelf stress had been occurring for years prior to the breakup [*Glasser and Scambos*, 2008; *Vieli et al.*, 2007; *Khazendar et al.*, 2007] and may have played a role in preconditioning Larsen B for collapse. For WIS, proposed collapse mechanisms include ocean surface wave action [*Massom et al.*, 2008; *Bromirski et al.*, 2010], ice-front bending coupled with the presence of a brine layer within the ice shelf [*Vaughan et al.*, 1993; *Scambos et al.*, 2009], changing internal stresses [*Humbert and Braun*, 2008; *Braun et al.*, 2009], and waves generated by the toppling bergs formed during the disintegration event itself (leading to a run-away breakup after a chance calving) [*MacAyeal et al.*, 2008].

[7] While there are many proposed mechanisms to explain the final stage of ice-shelf collapse events, there are few studies investigating the mass balance of ice shelves in the years leading up to their collapse. In this article, we examine the evolution of WIS mass balance during the decades prior

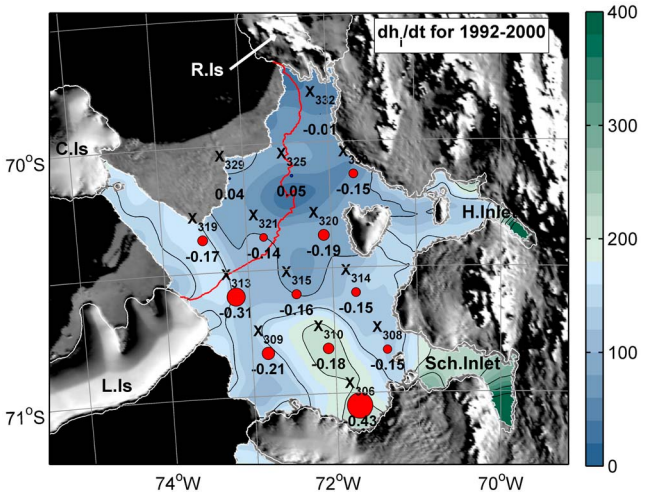

Figure 2. WIS ice draft (m; color scale on right) based on ERS geodetic mission data (1994–1995) adjusted to epoch 2008 based on measured surface elevation changes at crossovers. Maximum draft is ~380 m. Black contours are at 50 m intervals. Circles labeled X_{nnn} show mean surface elevation trends dh_i/dt (black text, values in m a^{-1}) for the period 1992–2000 at ERS-1/2 crossovers. Circle radii are scaled to trend magnitude; blue and red show increasing and decreasing elevation, respectively. Charcot, Latady, and Rothschild islands are indicated by "C.Is," "L.Is," and "R.Is," respectively. Haydn and Schubert inlets ("H.Inlet and Sch.Inlet") are indicated. Background is the Moderate Resolution Imaging Spectroradiometer (MODIS) Mosaic of Antarctica (MOA [*Scambos et al.*, 2007]) based on cumulation of multiple images from austral summer 2003/2004.

to the 2008–2009 collapse events, specifically to identify environmental factors that might influence rapid collapses of other portions of WIS and similar ice shelves. We first provide some background on the setting and structure of WIS (section 2) and then estimate the magnitudes of principal terms in the WIS mass balance (section 3) including basal melting, flux divergence, and accumulation for the period 1992–2008. We then present data that describe the climatic environment (ocean, sea ice, and atmosphere) of the region surrounding WIS (section 4). The results from sections 3 and 4 lead us to put forward a hypothesis that changes in WIS mass balance before the calving events are determined primarily by changes in basal melt rate and that, as most of the WIS ice base is relatively shallow (mean depth < 200 m), basal melting is sensitive to variability in upper-ocean hydrography and local circulation (section 5). We expect that this conclusion is valid for many ice shelves that are sufficiently thin for their bases to be sitting in water masses modified by local surface processes.

2. Background

[8] The WIS is one of two large ice shelves on the sBS continental shelf, the other being George VI Ice Shelf (GVIIS), which occupies the narrow, deep channel between Alexander Island and the AP (Figure 1). Both ice shelves lie at the inshore end of glacial troughs cutting across the sBS continental shelf [*Padman et al.*, 2010; *Graham et al.*, 2011]. Such troughs, in both the Bellingshausen and Amundsen seas, are known to be conduits for deep onshore flows of warm Circumpolar Deep Water (CDW) originating from the Antarctic Circumpolar Current offshore of the continental shelf break [*Dinniman and Klinck*, 2004; *Walker et al.*, 2007; *Thoma et al.*, 2008].

[9] The sBS continental shelf experiences significant interannual variability in atmospheric conditions [e.g., *Jacobs and Comiso*, 1997; *Lachlan-Cope and Connolley*, 2006]. This variability forces changes in sea-ice concentration [e.g., *Stammerjohn et al.*, 2008] and modeled ocean response [*Holland et al.*, 2010]. The latter study, which focused on temporal variability of modeled basal melt rates for GVIIS, found that the melt rate averaged over GVIIS ($\langle w_b \rangle$) responded to these interannual changes in the environment; modeled $\langle w_b \rangle$ varied by a factor of ~3, from ~1.5 to ~4 m a^{-1} (with a mean of ~2.5 m a^{-1} for 1979–2007). These authors also found a positive trend in $\langle w_b \rangle$ for these three decades; since 1989, $\langle w_b \rangle$ has exceeded the rate of ~2 m a^{-1} that is required to balance ice-shelf mass increases from surface mass balance (SMB; precipitation) and ice inflow from the grounded ice sheet on the AP and Alexander Island. The implied ice-shelf thinning since 1989 is generally consistent with estimates of surface elevation decrease for GVIIS based on satellite radar altimeter (RA) data for 1992–2002 [*Zwally et al.*, 2005].

[10] On the basis of these results, we expect that the mass balance of WIS will also experience interannual variability and a positive trend, driven by changes in SMB and ocean circulation (the latter responding to atmospheric variability and associated changes in sea-ice properties). However, model estimates of WIS basal melt are small. *Holland et al.*, [2010] obtained a mean value of 0.66 m a^{-1} for $\langle w_b \rangle$ for WIS, averaged over 1979–2007. M. S. Dinniman et al. (The influence of surface winds on Circumpolar Deep Water transport and ice shelf basal melt along the west Antarctic Peninsula, submitted to *Journal of Climate*, 2011) obtained $\langle w_b \rangle \approx 0.5$ m a^{-1} for 2000–2002. These values are about one-fourth of the long-term mean value for GVIIS. The difference may be due, in part, to ice-shelf thickness; the ice draft h_d for much of WIS is lesser than 200 m [*Braun et al.*, 2009] whereas GVIIS has an extensive region with h_d greater than 300 m and a maximum value of ~500 m [*Holland et al.*, 2010, Figure 1]. However, [*Zwally et al.*, 2005] found that the surface elevation loss for WIS for 1992–2002 was similar to that for GVIIS, suggesting that the nonequilibrium basal melt rate (the value above that required to balance other terms in the ice-shelf mass budget) might be similar for both ice shelves. This result raises the possibility that the modeled values of $\langle w_b \rangle$ for WIS are too low and motivates our search for mechanisms responsible for changes in WIS mass balance.

3. WIS Mass Balance

[11] Our first step is to determine whether the model-based estimates of $\langle w_b \rangle$ for WIS are realistic. As no direct measurements of $\langle w_b \rangle$ are available for WIS, we use an ice-shelf mass balance equation (section 3.1) to derive $\langle w_b \rangle$ as the residual of the other terms in the balance. The determination of each term is explained in sections 3.2–3.7.

3.1. Ice-Shelf Mass Balance Equation

[12] Repeated measurement of the surface elevation (h_i) of an ice shelf allows estimation of its geodetic mass balance [*Cox and March*, 2004]. The European Space Agency (ESA) RA satellites have measured surface elevation along repeated ground tracks since 1992, providing a 19 year time series. Other satellite missions have also measured h_i, including Seasat RA in 1978 [*Brooks et al.*, 1983; *Fricker and Padman*, 2012] and the laser altimeter on the Ice, Cloud, and land Elevation Satellite from 2003 to 2009 [*Yi et al.*, 2011].

[13] We express the mass balance of WIS in terms of the observed time rate of change of h_i, following *Shepherd et al.* [2003, 2004]:

$$\frac{\partial h_i}{\partial t} = \frac{\partial \Delta_s}{\partial t} - M\frac{\partial}{\partial t}\left(\frac{1}{\rho_w}\right) + \int_0^M \mathrm{d}m \frac{\partial}{\partial t}\left(\frac{1}{\rho_f(m)}\right) + \left(\frac{1}{\rho_i} - \frac{1}{\rho_w}\right)\left(\dot{M}_s + \dot{M}_b + \mathbf{u}_i \cdot \nabla M + M\nabla \cdot \mathbf{u}_i\right). \quad (1)$$

[14] In equation (1), Δ_s is the sea level height (m); M is the ice-shelf mass per unit area (kg m^{-2}); ρ_w, ρ_i, and ρ_f are the densities of water, ice, and firn, respectively (kg m^{-3}), $\dot{M}_s$ and $\dot{M}_b$ are the rates of surface and basal accumulations of ice (kg m^{-2} s^{-1}), and u_i is the horizontal ice velocity (m s^{-1}). The terms on the right-hand side of equation (1) are ice-shelf height changes because of (in order): (1) sea level variations including mass and steric changes associated with dynamic ocean topography and ocean tides, (2) ocean density changes that affect the elevation of hydrostatically balanced ice, (3) firn compaction, (4) surface and basal accumulation rates, and (5) thickness changes caused by advection of thickness gradients and flow divergence. The last two terms are the expansion of the mass flux divergence "$\nabla \cdot (M\mathbf{u}_i)$" term given in the study by *Shepherd et al.*

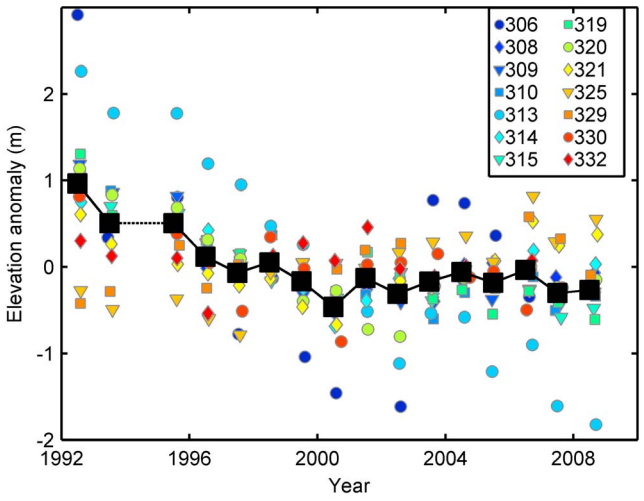

Figure 3. Time series of annual-averaged (winter only) surface elevation anomaly (relative to mean elevation) at the 14 orbital crossovers on WIS, following the methodology of *Fricker and Padman* [2012]; see Figure 2 for crossover locations. Elevations have been corrected for ocean tide and ocean tide loading, and for constant surface slope at the nominal crossover location. Black symbols show the mean anomaly for all 14 crossovers.

[2004], the correction to the form of the equation published by *Shepherd et al.* [2003]. Equation (1) only applies to the portion of the floating shelf that is in hydrostatic balance, not to the flexural boundary layer along the ice-shelf grounding zone [see e.g., *Fricker and Padman*, 2006].

3.2. Ice-Shelf Surface Elevation (h_i) Changes From Satellite Radar Altimetry

[15] Following the studies by *Zwally et al.* [2005] and *Fricker and Padman* [2012], we used RA data from the 35 day repeat phases of ESA's ERS-1, ERS-2, and Envisat satellites to determine time series of annual-averaged h_i for the period 1992–2008, at 14 "crossover" locations (i.e., where ascending and descending ground tracks intersect) [*Zwally et al.*, 1989] on WIS (see Figure 2 for locations). To avoid potentially significant changes in radar penetration depth [*Helsen et al.*, 2008], we used only measurements acquired between 1 April and 30 November each year (i.e., excluding the summer melt season). We also calculated a surface slope correction to account for sampling of spatial variability of h_i as the exact location of crossovers varies with time [see *Fricker and Padman*, 2012, Appendix]. Figure 3 shows the time series of RA-derived annual-averaged (non-summer) elevation anomalies at these crossovers.

[16] The WIS experienced significant mean surface lowering between the Seasat era in 1978 and the start of modern, quasi-continuous satellite altimeter operations in 1992 [*Fricker and Padman*, 2012]. This lowering continued until about 2000 (see Figure 3), after which $\mathrm{d}h_i/\mathrm{d}t \approx 0$ at most WIS crossovers. The exception to this behavior was at crossover X_{313} (see Figure 2) near the eastern end of Latady Island, where the surface continued to lower through 2008.

[17] The linear trends of $\mathrm{d}h_i/\mathrm{d}t$ for epoch 1992–2000 at each RA crossover on WIS (Figure 2) varied from slightly positive ($\mathrm{d}h_i/\mathrm{d}t$ = +0.04–0.05 m a^{-1}) over the northern WIS at crossovers marked X_{325} and X_{329} to strongly negative ($\mathrm{d}h_i/\mathrm{d}t \approx -0.43$ m a^{-1}) at crossover X_{306}, near the grounding line in the south. Crossover X_{313} also experienced rapid lowering ($\mathrm{d}h_i/\mathrm{d}t \approx -0.31$ m a^{-1}) during this period. The mean value for the 14 crossovers on WIS for 1992–2000 was $\langle \mathrm{d}h_i/\mathrm{d}t \rangle \approx -0.15$ m a^{-1}. For the period 2001–2008, the average value of $\langle \mathrm{d}h_i/\mathrm{d}t \rangle$ for WIS was close to 0.

3.3. Ice-Shelf Thickness and Ice Draft (H and h_d)

[18] We estimated ice-shelf thickness H and ice draft h_d by assuming the ice shelf to be in hydrostatic equilibrium so that H can be determined from measured freeboard elevation and an ice density model. We first developed a high-resolution digital elevation model (DEM) for the ice surface using along-track RA data from the ERS-1 geodetic mission, phases E and F, conducted in 1994–1995 [*Bamber and Bindschadler*, 1997; *Fricker et al.*, 2000]. The ERS-1 satellite flew in two offset 168 day repeat orbits during these phases, providing much denser track-to-track spacing than the usual 35 day orbit. We referenced tide-corrected RA elevation data to mean sea level (h_{MSL}) by applying a geoid correction from EGM2008 [*Pavlis et al.*, 2008], and a mean dynamic topography (MDT) correction of −1.4 m determined from nearby open-ocean elevations during sea-ice-free periods. Our method used to derive the epoch 1994–1995 DEM is generally consistent with that followed in the studies by *Bamber et al.* [2009] and *Griggs and Bamber* [2009] except for our inclusion of the MDT correction.

[19] To adjust our DEM to epoch 2008, we added the mean observed change in elevation averaged over all WIS crossovers between 1995 and 2008 (−0.8 m, see Figure 3) to all DEM values, then estimated H from

$$H = \frac{h_{\mathrm{MSL}} + h_f\left(\rho_f - \rho_i\right)}{\left(\rho_w - \rho_i\right)}, \qquad (2)$$

where h_f is the assumed thickness of the firn layer. Following the study by *Scambos et al.* [2009], we assume values of ρ_w, ρ_i, and ρ_f = 1028, 917, and 700 kg m^{-3}, respectively. The value of h_f at each grid node is taken as the minimum of 15 m and h_{MSL}; thus, we assume that there is no firn below the level of the sea surface. From this estimate we then obtained $h_d = H - h_{\mathrm{MSL}}$ (Figure 2) and ice mass density from $M = \rho_w h_d$ (kg m^{-2}).

3.4. Lateral Ice Velocity ($\mathbf{u}_i$)

[20] We determined the ice-shelf flow velocity $\mathbf{u}_i$ using a combination of interferometric synthetic aperture radar (InSAR) and speckle-tracking methods [*Joughin*, 2002] applied to data collected by the Japanese Space Agency's ALOS synthetic aperture radar from 2006 to 2008. Errors computed from the local image statistics are small (less than ~2 m a^{-1}) but larger errors may result from baseline errors, uncompensated tidal errors, and ionospheric effects [*Gray et al.*, 2000]. While it is difficult to evaluate these errors, they should generally be less than 10 m a^{-1}.

[21] Values of $\mathbf{u}_i$ for 2007 (Figure 4a) are lesser than 120 m a^{-1} over most of WIS, but with a few regions with $|\mathbf{u}_i|$ greater than 200 m a^{-1} at major glacier inflows around

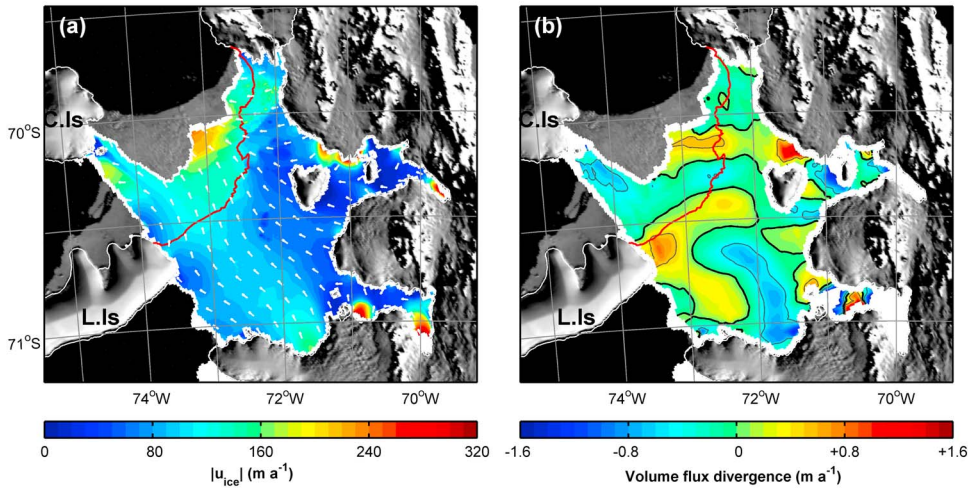

Figure 4. (a) Ice speed (shaded; m a^{-1}) and direction (white arrows) from 2007 Advanced Land Observing Satellite (ALOS) interferometric synthetic aperture radar (InSAR). White outline is ice-shelf extent from Mosaic of Antarctica [*Scambos et al.*, 2007], epoch 2003/2004. Red line is the location of the northern ice front in February 2011. (b) Mass divergence converted to ice-shelf thickness change (m a^{-1}) calculated from ice velocity and thickness fields smoothed over ~15 km. Bold black contour is zero divergence; lighter contours show ±0.5 m a^{-1}.

the WIS perimeter and along the northern portion of the ice shelf between Charcot and Rothschild islands.

3.5. Ice-Shelf Lateral Mass Divergence ($\nabla \cdot (M\mathbf{u}_i)$)

[22] We estimated the spatial distribution of ice mass divergence $\nabla \cdot (M\mathbf{u}_i)$ by combining the maps of $M(x,y)$ (section 3.3) and $\mathbf{u}_i(x,y)$ (section 3.4). We first smoothed each of $M(x,y)$ and $\mathbf{u}_i(x,y)$ to a length scale of ~15 km to reduce the impact of measurement errors. The resulting map of equivalent ice thickness change $\nabla \cdot (M\mathbf{u}_i)/\rho_i$ (Figure 4b) shows values in the range ±0.8 m a^{-1} over the main portion of WIS, with larger values near the tip of Latady Island and in Haydn and Schubert inlets (see Figure 2) where large glaciers enter from Alexander Island. The value of $\nabla \cdot (M\mathbf{u}_i)/\rho_i$ averaged over WIS is ~−0.2 m a^{-1}; that is, a weak mean thinning from ice flow divergence.

3.6. Surface Accumulation Rate ($\dot{M}_s$) and Surface Elevation From Atmospheric Processes

[23] The value of $\dot{M}_s$ for WIS has previously been estimated at ~500 kg m^{-2} a^{-1} [*Vaughan et al.*, 1993; *Arthern et al.*, 2006; *van de Berg et al.*, 2006]. We also obtained estimates of $\dot{M}_s$ from the Regional Atmospheric Climate Model (RACMO2) (J. T. M. Lenaerts et al., Modeling drifting snow in Antarctica with a regional climate model: 1. Methods and model evaluation, submitted to *Journal of Geophysical Research*, 2011). This model is forced at the lateral boundaries by the ERA-Interim [*Dee et al.*, 2011] global atmospheric reanalysis and has a horizontal grid spacing of 27 km. We report model output for 1979–2010 from a single grid cell centered near 70.5°S, 72.5°W, the center of WIS. For this location, the annual total precipitation ranges from ~400 to 900 kg m^{-2}, with a mean value of 620 kg m^{-2} (Figures 5a and 5b). The linear trend for 1979–2010 is not significantly different from zero. For the remainder of this article, we assume that the value of $\dot{M}_s$ for WIS is 650 ± 250 kg m^{-2} a^{-1}, which encompasses the full range of both measured and modeled values. Equivalent ice thickness rate of change is $\dot{M}_s/\rho_i \approx 0.7 \pm 0.3$ m a^{-1}.

[24] A firn densification model forced with RACMO2 output provides estimates of surface elevation changes caused by changes in the depth of the firn layer owing to snowfall, melting, and firn compaction [*Ligtenberg et al.*, 2011]. The model corrects for buoyancy effects on ice shelves and provides surface elevation changes at the ice-shelf surface that are solely caused by surface and firn layer processes relative to zero mean for the period 1979–2010. The time series of this elevation, $h_{i,s}$, for WIS (Figure 5c) shows seasonal variability and a large interannual signal with a total range of ~1 m when firn layer density variations are included and a smaller but still significant range when only precipitation changes are considered. As firn compaction is a steady process with relatively low interannual variability [*Ligtenberg et al.*, 2011], the difference between the two is caused mainly by interannual variability in snowmelt. For instance, the summers of 1980–1981 and 2000–2001 had almost no melt on WIS.

3.7. Basal Accumulation Rate ($\dot{M}_b$)

[25] The basal accumulation rate $\dot{M}_b$ is determined as the residual of other terms in equation (1); therefore, errors in $\dot{M}_b$ represent the accumulation of errors in all mass balance terms. For consistency with other studies of ocean/ice-shelf interactions, we also define a basal melt rate, w_b (m s^{-1}) as:

$$w_b = -\frac{\dot{M}_b}{\rho_i} \text{ m s}^{-1}. \quad (3)$$

[26] A positive value of w_b implies melting; $w_b < 0$ implies marine ice accretion to the base. We used equation (1) to estimate $\dot{M}_b$ from dh_i/dt for the two periods 1992–2000 ("thinning") and 2001–2008 ("steady state"). We assume that the contributions to ice thickness variability from sea

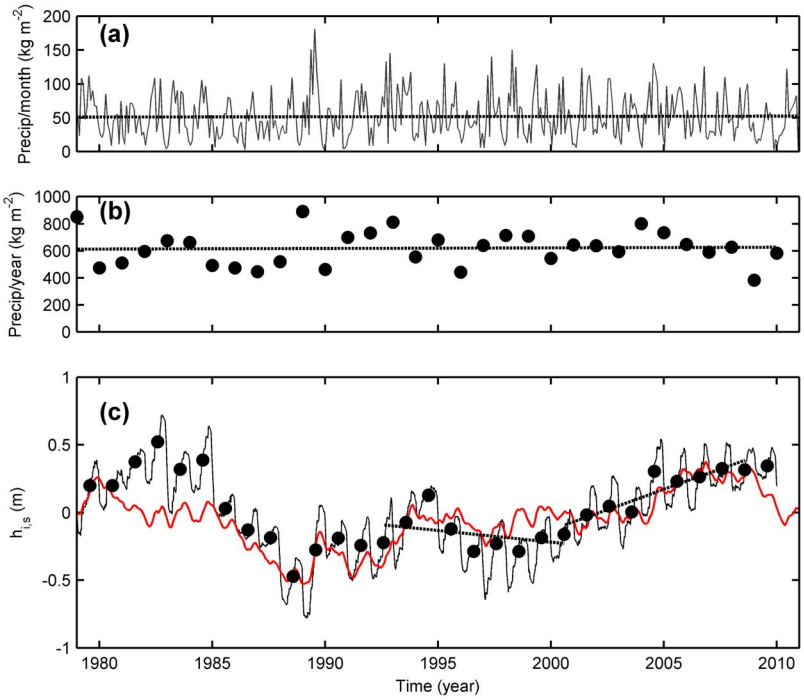

Figure 5. (a) Monthly values of precipitation (kg m^{-2}) from the Regional Atmospheric Climate Model (RACMO2) (see section 3.6) for a grid cell near the center of WIS (70.5°S, 72.5°W). The linear trend is shown by a dashed line; the trend is not significantly different from zero. (b) Annual total precipitation (kg m^{-2}) from the same source. The linear trend is shown by a dashed line; the trend is not significantly different from zero. (c) Time series of daily surface elevation relative to zero mean (solid black line) for the period 1979–2010, based on a firn densification model forced by RACMO2 output and considering only surface processes. Red line shows elevation based on cumulative ice-equivalent (ρ_i = 917 kg m^{-3}) surface mass balance (SMB) anomaly relative to series mean. Filled circles show annual averages for 1 April to 30 November (nonsummer) each year. Dashed lines show trends for 1992–2000 (−0.017 m a^{-1}) and 2001–2008 (+0.060 m a^{-1}), the periods identified from radar altimetry as surface lowering and steady state, respectively (see Figure 3).

level and ocean density changes are negligible, justifying these assumptions as follows:

[27] 1. Change in sea level Δ_s from dynamic ocean topography and global sea level rise is less than 0.1 m, based on a time series of monthly sea surface height (SSH) (Figure 6) measured by coastal tide gauge at Verdansky (formerly Faraday) Station (see Figure 1 for location). This is the nearest long-duration, in situ SSH record to WIS.

[28] 2. Seawater density varies less than 0.2%, and so has a negligible effect on dh_i/dt.

[29] Furthermore, we assume that ice-shelf mean lateral divergence $\nabla \cdot (M\mathbf{u}_i)$, which is calculated from ice velocities measured in 2006–2008, late in the analysis period (see section 3.4), is constant (and small) throughout the period 1992–2008. It is possible, however, that $\nabla \cdot (M\mathbf{u}_i)$ changes during that time, perhaps as a response to the preceding large calving event in 1990/1991 [*Braun et al.*, 2009].

[30] We take two approaches to modeling the firn compaction term in equation (1). In the first, we assume that trends in h_i, solely because of surface processes including precipitation and firn compaction (denoted $h_{i,s}$), are small. We base this model (d$h_{i,s}$/dt = 0) on the lack of long-term trends in the SMB (Figures 5a and 5b) and the observation that there has been an extensive (∼90–100 day) summer melt season for WIS almost every summer over the period considered here (approximately from 1978); thus, snowfall should be routinely transformed to ice by melt and refreezing through each summer. Recent studies in the northern Larsen C ice shelf demonstrate that long melt seasons lead to denser firn [*Holland et al.*, 2010]. Moreover, the presence of melt ponds on the WIS surface in some summers [*Vaughan*

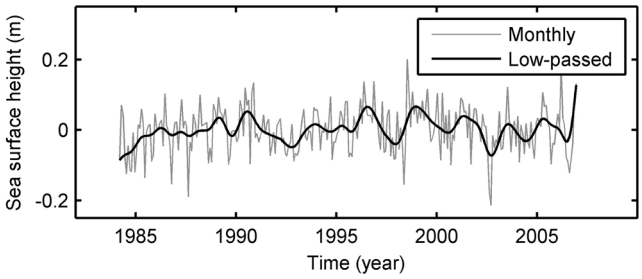

Figure 6. Time series of sea surface height (SSH) measured by tide gauge at Verdansky (formerly Faraday) Station on the western side of the northern Antarctic Peninsula (see Figure 1 for location). Gray line is monthly average SSH; bold black line has been low-passed at a period of 15 months to emphasize interannual variability.

et al., 1993; *Lucchitta and Rosanova*, 1998] indicates dense, impermeable firns.

[31] In the second approach, we use our firn densification model based on the RACMO2 atmospheric model to estimate temporal changes in $h_{i,s}$. Figure 5c shows the time series of $h_{i,s}$ from 1979 to 2010, adjusted to zero mean for that period. Even though the long-term trend in $\dot{M}_s$ is negligible (Figures 5a and 5b), there is significant interannual variation in the time series of buoyancy-adjusted elevation because of the cumulative precipitation anomaly and changes in snowfall melting (Figure 5c). For the two epochs identified by distinct trends in RA measurements of h_i, 1992–2000 and 2001–2008 (Figure 3), the linear trends of the modeled contribution from $h_{i,s}$ are $\mathrm{d}h_{i,s}/\mathrm{d}t = -0.017$ and $+0.060$ m a^{-1}, respectively.

[32] With the simplifications discussed previously, equation (1) can be rewritten as:

$$\dot{M}_b = \left(\frac{\mathrm{d}h_i}{\mathrm{d}t} - \frac{\mathrm{d}h_{i,s}}{\mathrm{d}t}\right)\left(\frac{1}{\rho_i} - \frac{1}{\rho_w}\right)^{-1} - \dot{M}_s - \nabla \cdot (M\mathbf{u}_i). \quad (4)$$

[33] To evaluate $\dot{M}_b$ from equation (4), we use $\rho_w = 1028$ kg m^{-3} and $\rho_i = 917$ kg m^{-3} [*Scambos et al.*, 2009], an ice-shelf-averaged value of $\dot{M}_s = 650 \pm 250$ kg m^{-2} a^{-1} (section 3.6), and divergence of -200 kg m^{-2} a^{-1} (section 3.5). With these values, an area-averaged value of $\mathrm{d}h_i/\mathrm{d}t = -0.15$ m a^{-1} (epoch 1992–2000) with $\mathrm{d}h_{i,s}/\mathrm{d}t = 0$ implies $\dot{M}_b \approx -(1.5 - 2.0) \times 10^3$ kg m^{-2}a^{-1}, corresponding to a basal melt rate of $w_b = 1.9 \pm 0.3$ m a^{-1} (equation 3). Using $\mathrm{d}h_{i,s}/\mathrm{d}t = -0.017$ m a^{-1} (from Figure 5c), we obtain $w_b = 1.7 \pm 0.3$ m a^{-1}.

[34] For epoch 2001–2008, where $\mathrm{d}h_i/\mathrm{d}t \approx 0$ m a^{-1}, we obtain $w_b = 0.5 \pm 0.3$ m a^{-1} and 1.0 ± 0.3 m a^{-1} for $\mathrm{d}h_{i,s}/\mathrm{d}t = 0$ and $+0.060$ m a^{-1}, respectively. That is, depending on the SMB model we use, w_b decreases by a factor of between 2 and 4 from 1992–2000 to 2001–2008. We incorporate the uncertainty in the choice of SMB model into the error estimates for $\dot{M}_b$ for each epoch, resulting in values of $w_b = 1.8 \pm 0.4$ m a^{-1} and 0.75 ± 0.55 m a^{-1} for 1992–2000 and 2001–2008, respectively.

[35] While we have performed the mass balance calculations presented here on ice-shelf-averaged values, there is a significant spatial variation in estimated $\dot{M}_b$. The small amount of thickening observed at crossovers X_{325} and X_{329} on the northern ice shelf (Figures 2 and 3) for 1992–2000 is consistent with surface accumulation exceeding basal melt plus divergence there. We do not expect basal accumulation from the formation of marine ice [see e.g., *Fricker et al.*, 2001; *Joughin and Padman*, 2003; *Holland et al.*, 2009] under WIS because there is no evidence of potentially supercooled ice-shelf water (i.e., water with potential temperature $\theta < T_{\mathrm{freeze}}(P = 0)$) anywhere in the vicinity. For crossover X_{313} (Figure 2), with $\mathrm{d}h_i/\mathrm{d}t \approx -0.31$ m a^{-1} during 1992–2000 and divergence of $+0.5$ m a^{-1} (Figure 4b), the estimated value is $w_b = 4.1 \pm 0.3$ m a^{-1}.

4. Environmental Setting

[36] The WIS mass balance responds primarily to oceanic and atmospheric forcing; inflow from grounded glaciers is small [*Vaughan et al.*, 1993; *Braun et al.*, 2009]. In this section, we summarize the environmental setting using the following: regional distribution of ocean temperature mapped by instrumented seals (section 4.1), sea-ice concentration as the longest continuous record of environmental change over the sBS (section 4.2), and meteorological conditions (air temperature and wind speed and direction) derived from an atmospheric model (section 4.3).

4.1. Regional Hydrography

[37] An extensive set of hydrographic data (profiles of temperature T, conductivity C, and derived salinity S as functions of depth D) has been compiled by the Palmer Long-Term Ecological Research (LTER) program that has collected data from 1993 to the present [*Martinson et al.*, 2008], and by the Southern Ocean (SO) Global Ocean Ecosystems Dynamics (GLOBEC) program in 2001–2002 [*Klinck et al.*, 2004; *Costa et al.*, 2008]. However, most of these measurements were acquired in Marguerite Bay and the Bellingshausen Sea continental shelf north of WIS. For the portion of the sBS continental shelf south of Marguerite Bay, the only published hydrographic data are from a cruise in 1994 [*Jenkins and Jacobs*, 2008]. These data provide important information on the broad hydrographic structure of the region, specifically close to the GVIIS northern and southern ice fronts, but do not provide a detailed map of hydrography near WIS.

[38] An alternative source of hydrography data is now available; satellite-telemetered measurements from instrumented marine mammals including seals. These data have been acquired to investigate migration, foraging, and other animal behavior [e.g., *Burns et al.*, 2004; *Biuw et al.*, 2007; *Costa et al.*, 2010]. Recent studies have also demonstrated the value of the measurements for physical oceanographic studies in regions with few or no standard ship-based measurements [e.g., *Charrassin et al.*, 2008; *Nicholls et al.*, 2008; *Costa et al.*, 2010; *Williams et al.*, 2011].

[39] We used data obtained from a total of 38 southern elephant seals (*Mirounga leonina*) that were instrumented with conductivity-temperature-depth Satellite Relay Data Loggers (CTD-SRDLs, or "tags") in 2007 (12 seals), 2008 (12 seals), and 2009 (14 seals) after molting at the Cape Shirreff rookery on Livingston Island in the South Shetland Islands, Antarctica. These seals made numerous dives over a broad region of the sBS between February and September of each year (Figure 7). Approximately 30% of the dives over the continental shelf were to the seabed [*Padman et al.*, 2010]. Further information on acquisition and initial processing of these data is provided in Appendix A.

[40] The vertical structure of temperature, $T(z)$, surrounding WIS varies spatially (Figure 8), but the same principal water masses are usually present. The late summer profiles obtained from instrumented seal dives (e.g., Figures 8a and 8b) show a surface layer of relatively warm (and fresh; not shown) Antarctic Surface Water (AASW) that is generated by insolation and sea-ice melt during summer. The underlying cold layer, denoted "Winter Water" (WW), is the residual stratification from convective cooling, brine input from sea-ice formation, and deepening of the surface mixed layer during the preceding winter. This layer extends up to the sea surface in SO GLOBEC CTD profiles obtained north of WIS in austral winter (e.g., Figure 8c). The bottom of the WW layer is much deeper near WIS (Figure 8b) than over

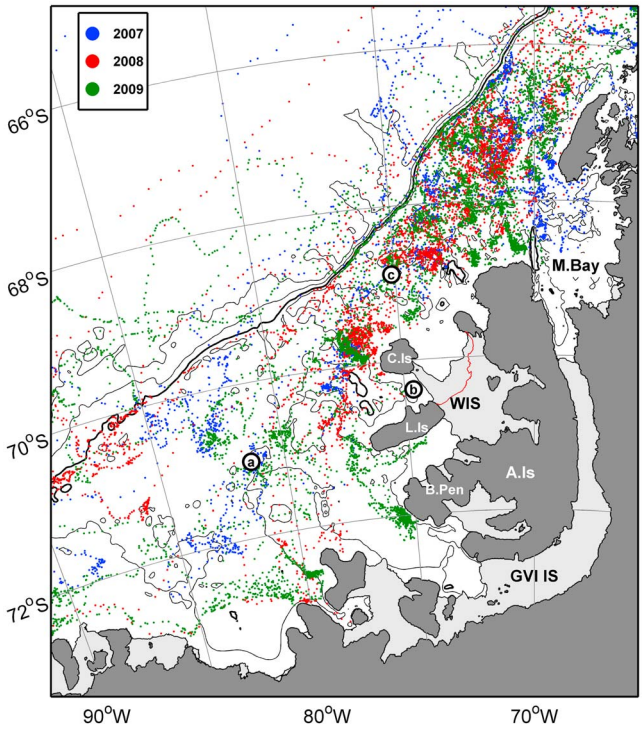

Figure 7. Seal-dive locations for 2007–2009, color-coded by year. Contours indicate 500, 1000, 2000, and 3000 m isobaths from TOPO 11.1 bathymetry grid. Black circles denoted "a" (near 71°S, 81°W) and "b" (near 70.5°S, 75°E, between Charcot and Latady islands (C.Is and L.Is)) indicate locations of the seal-dive temperature profiles shown in Figures 8a and 8b. Black circle denoted "c" (near 69°S, 75°W) shows location of Southern Ocean Global Ocean Ecosystems Dynamics conductivity-temperature-depth temperature profile shown in Figure 8c.

the central continental shelf (Figures 8a and 8c). Below the WW, a thermocline extends downward to the top of the Upper Circumpolar Deep Water (UCDW) near 250–400 m depth. The UCDW layer, which extends to the seabed, is relatively uniform in $T(z)$.

[41] The ice draft for most of WIS is in the range 80–260 m (Figure 2), with an estimated mean value of ~170 m (epoch 2008; see section 3.3). Maximum ice draft is ~400 m at the grounding lines of the major glaciers flowing off Alexander Island through Haydn and Schubert inlets. We use the distribution of mean maximum temperature T_{max} in the UCDW layer (considering only measurements below 350 m), and the distribution of mean temperature near 180 m depth, T_{180}, as guides to the temperature of water masses that might influence w_b under WIS. Both values were evaluated from all seal CTD-SRDL tags for 2007–2009 in nonoverlapping 20 × 20 km boxes. The value T_{180} was obtained by averaging all temperature values recorded between depths of 155 and 205 m (i.e., 180 ± 25 m), chosen to approximate water near the estimated mean ice draft of WIS over the period of RA measurements reported here (1992–2008).

[42] The UCDW temperature (T_{max}) exceeds 1.0°C over almost the entire sBS continental shelf (Figure 9a). The UCDW over the continental shelf north of the northern extent of Alexander Island and including Marguerite Bay is slightly warmer (~1.5°C) than to the west and south of WIS. These seal-derived values are generally consistent with ship CTD measurements from SO GLOBEC [*Klinck et al.*, 2004]. Values of T_{max} greater than 2°C offshore of the shelf break mark the presence of the Antarctic Circumpolar Current, the offshore source of UCDW intrusions onto the continental shelf [*Dinniman and Klinck*, 2004]. There is a region of relatively cool T_{max} (<1°C) extending from north of Charcot Island to the northern coast of Alexander Island.

[43] For all grid boxes south of Marguerite Bay, T_{180} (Figure 9b) is much lower than T_{max} (Figure 9a). A band (or "halo") of T_{180} lesser than 0°C surrounding WIS is reminiscent of the Antarctic Peninsula Coastal Current (APCC) described by *Moffat et al.* [2008]. Those authors identified the APCC in oceanographic moorings along the coast of Adelaide Island north of Marguerite Bay and concluded that the APCC is a seasonal (summer/fall) current that is driven by summer freshwater input from melting land ice and sea ice, combined with coastal downwelling associated with the generally southward wind stress along the coast [see also *Hyatt et al.*, 2011]. The cooled water near 180 m depth around WIS may also contain a significant component of meltwater from the WIS and GVIIS bases [*Dorland and Zhou*, 2008; *Jenkins and Jacobs*, 2008]. We expect the contribution to ocean cooling of basal melt from WIS and GVIIS to be most pronounced in the upper ocean as the ice-shelf-modified water is fresher (and, therefore, also lighter) than the source water. Some cooling of the UCDW layer may occur through enhanced mixing between UCDW and the overlying cooler thermocline. Although we have not yet identified any mechanisms that might be responsible for such deep mixing in this region [*Howard et al.*, 2004], we note that variability of mixing on seasonal and interannual time scales may influence the vertical distribution of water masses over the continental shelf [*Holland et al.*, 2010].

[44] Although the water at 180 m depth close to WIS is much cooler than the UCDW layer, it is still significantly warmer than the in situ freezing point (see Figure 8b), and so is capable of inducing ice melt if it can penetrate the sub-ice-shelf cavity.

4.2. Sea-Ice Concentration (C_{ice})

[45] The hydrographic information from the instrumented seals is only available since 2006, during the period of negligible surface elevation change over most of WIS (Figure 3); however, we seek to identify potential causes of the transition in WIS basal melt rate around the year 2000. The longest continuous record of environmental change for the sBS continental shelf is provided by passive microwave radiometers on satellites [*Cavalieri and Parkinson*, 2008]. We obtained daily sea-ice concentration (C_{ice}) maps from the National Snow and Ice Data Center data set of Special Sensor Microwave/Imager (SSM/I) products (http://nsidc.org/data/seaice/pm.html) [*Cavalieri et al.*, 1996] from the Defense Meteorological Satellite Program satellites for the period 1 January 1980 to 31 December 2010. These data are provided on a 25 km grid, with land and ice shelves masked out. We use data processed with the "NASA Team 1" algorithm [*Cavalieri et al.*, 1984].

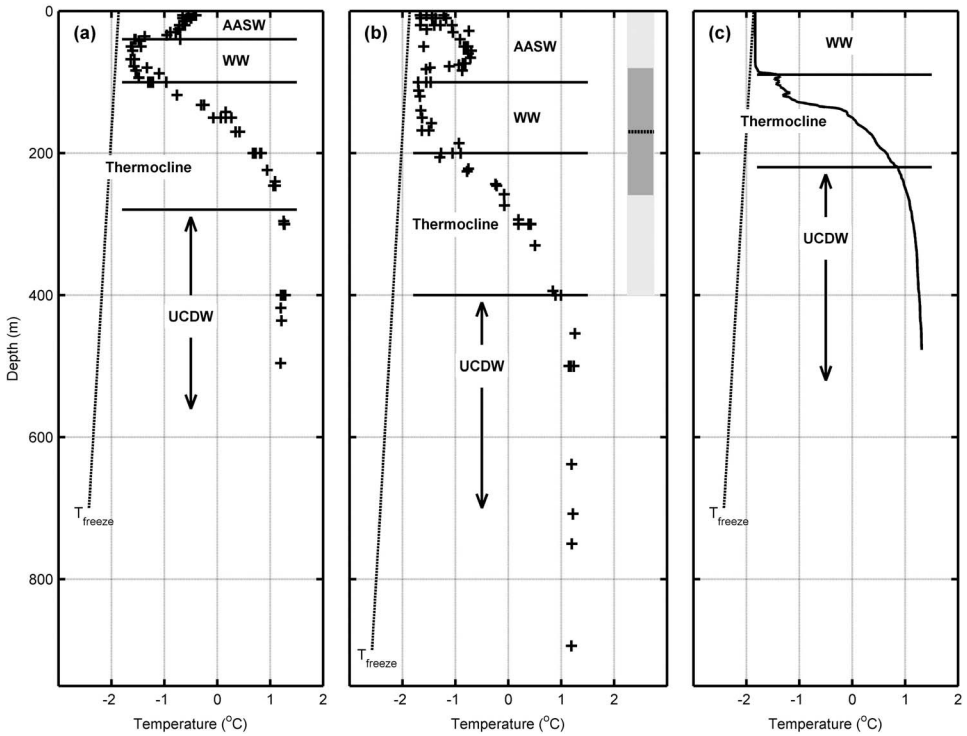

Figure 8. Vertical profiles of temperature obtained in three locations around WIS, indicated on Figure 7: (a) The midcontinental shelf west of WIS; (b) the passage between Charcot and Latady islands; and (c) north of WIS. The first two profiles were obtained by instrumented seals in February and March (late summer) 2008. The third profile comes from a Southern Ocean Global Ocean Ecosystems Dynamics conductivity-temperature-depth survey in August (winter) 2002. Depth ranges of water masses are indicated: Antarctic Surface Water (AASW); Winter Water (WW); Upper Circumpolar Deep Water (UCDW); and the thermocline separating WW from UCDW. The dashed line shows the approximate pressure-dependent melting point temperature for a typical salinity profile in this region. The gray rectangle on the right side of Figure 8b shows approximate depth range of ice draft; light gray is full range, dark gray is majority of ice shelf ($80 < h_d < 260$ m) and dashed line is ice-shelf-averaged h_d for epoch 2008.

[46] While grids of C_{ice} at higher spatial resolution are now available from the Advanced Microwave Scanning Radiometer–EOS (AMSR-E) sensor on NASA's Aqua satellite, these data were not collected before May 2002. For consistency with the period of the RA record (1992–2008), we used only the SSM/I data set.

[47] The time-averaged value of C_{ice} (denoted $\langle C_{ice} \rangle_t$) around WIS (Figure 10a), evaluated as the mean of the daily gridded values for the period 1980–2008, exceeds 60% over most of the sBS continental shelf. Slightly lower values (~50%) are found close to the coast and ice fronts including in the channel between Latady Island and Beethoven Peninsula.

[48] The daily time series of C_{ice}, averaged spatially over an area of ~200 × 200 km on the western side of WIS (for location of averaging domain, see Figure 10) shows the expected annual cycle as well as significant interannual variability (Figure 11a); [see also *Holland et al.*, 2010, Figure 4]. During most winters, C_{ice} exceeds 80% for several months. Summer minima vary from 0% in some years to greater than 60% in others. Prior to 1989, a typical summer minimum in area-averaged C_{ice} was ~60%: Since 1989, most summers have had minima of 20%–40%, with the exception of 2004/2005 and 2005/2006 (which had minima of ~60%).

[49] *Stammerjohn et al.* [2008] estimated the duration of the ice-free ("summer") season in the Bellingshausen Sea, for each 25 × 25 km SSM/I pixel, from the number of days per year with C_{ice} less than 15%. They found that the duration increased during the period 1992–2004. Our analyses indicate that the longer-term trend (1979–2008) in the vicinity of WIS is dominated by the transition in 1989 rather than by a steady trend (Figure 11a). The largest changes occur along a region from offshore the continental shelf near 90°W to the entrance to Marguerite Bay, roughly following the contour of $\langle C_{ice} \rangle_t = 60\%$ (Figure 10b).

4.3. Meteorology

[50] There are no sources of in situ meteorological data close to WIS. The nearest automatic weather stations (AWSs) are two short-duration stations located to the north of WIS in Marguerite Bay (Dismal and Kirkwood islands) [*Hyatt et al.*, 2011], and at 780 m elevation on Uranus Glacier on the eastern side of Alexander Island (see Figure 1 for locations). Therefore, instead of direct measurements,

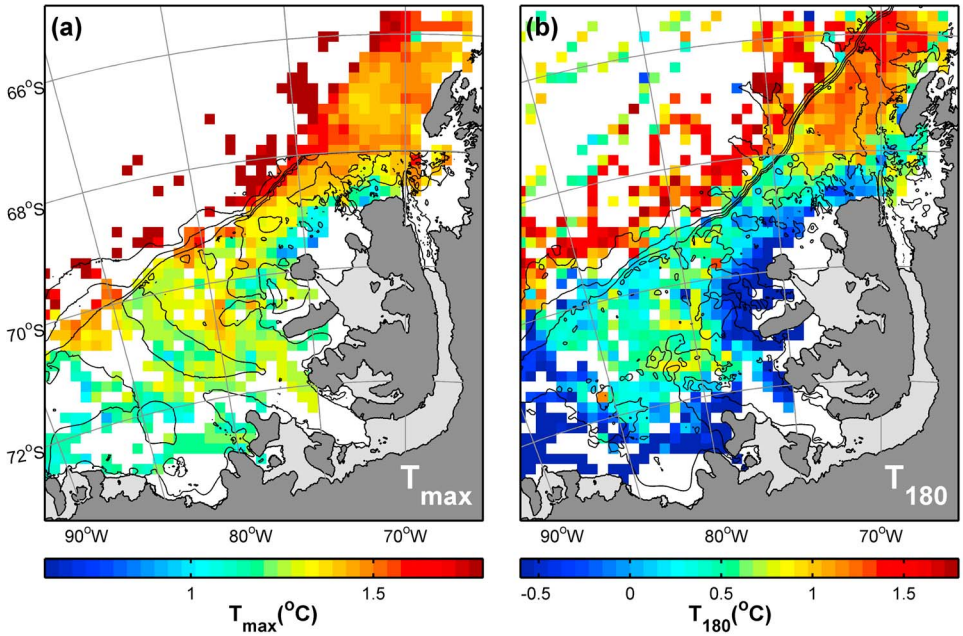

Figure 9. Maps of temperature recorded by conductivity-temperature-depth Satellite Relay Data Loggers on instrumented seals during 2007–2009, evaluated in nonoverlapping 20 × 20 km boxes: (a) Mean maximum temperature (T_{max}) at depths below 350 m; (b) mean value of temperature in depth range 180 ± 25 m (T_{180}). Note different color scales for Figures 9a and 9b. Only cells with data in them have been colored; there is no interpolation. Contours indicate 500, 1000, 2000, and 3000 m isobaths.

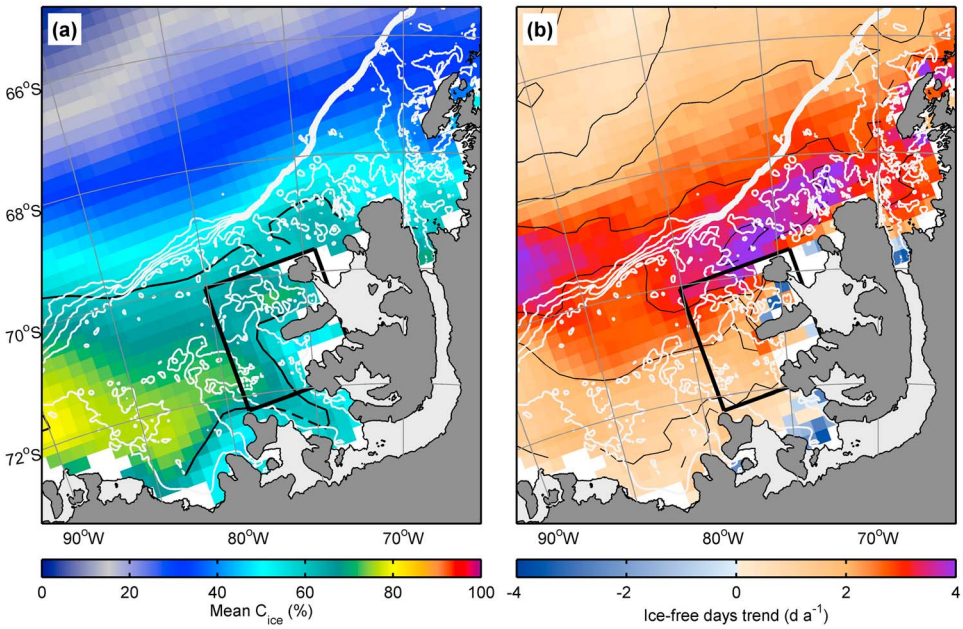

Figure 10. (a) Time-averaged mean sea-ice concentration $\langle C_{ice} \rangle_t$ (percent) from Special Sensor Microwave/Imager passive microwave (NASA Team 1 algorithm) for the period 1 January 1980 to 31 December 2008. Black contours are of $\langle C_{ice} \rangle_t$ = 60%. White contours are TOPO 11.1 bathymetry at 500 m intervals. Black rectangle to the west of WIS indicates the area used for spatial averaging of C_{ice} (see Figure 11a). (b) Trend, in days per year (d a^{-1}) in the duration of the "ice-free" summer season, defined as the number of days with C_{ice} < 15%. Black contours are at are at (1,2,3,4) d a^{-1}.

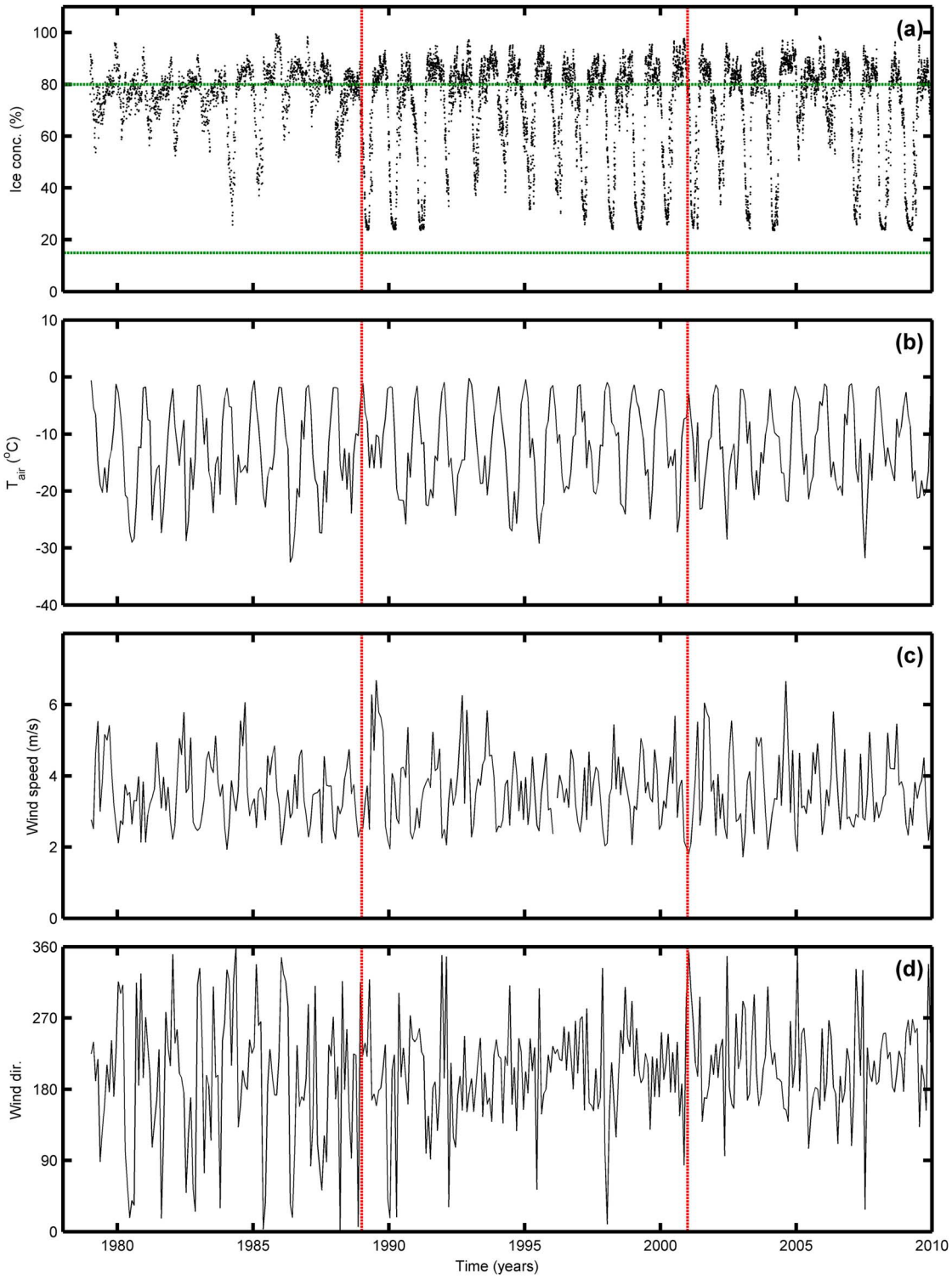

Figure 11. (a) Daily sea-ice concentration C_{ice} (percent), spatially averaged over the rectangle shown in Figure 10, for the period 1979–2010. Horizontal green dashed lines show C_{ice} = 15% and 80%. Vertical red dashed lines on all panels indicate starts of 1989 and 2001. Figures 11b–11d show time series of monthly averaged atmospheric parameters from the RACMO2 model (see section 3.6) for a single grid cell near the center of WIS. (b) Air temperature (°C) at 2 m; (c) 10 m wind speed (m s^{-1}); and (d) wind direction (°T) in oceanographic convention, that is, direction toward which the wind is blowing.

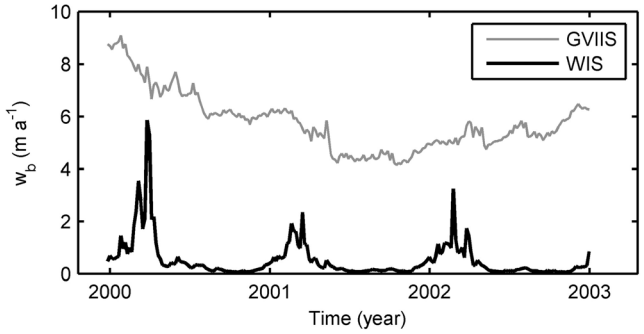

Figure 12. Time series of modeled ice-shelf-averaged basal melt rate for GVIIS and WIS, following the study by Dinniman et al. (submitted manuscript, 2011).

we used time series of atmospheric variables from the RACMO2 atmospheric model (see section 3.6).

[51] The time series of monthly averaged 2 m air temperature (T_{air}) over WIS from RACMO2 shows that, while the summer mean values were similar each year (~0°C), winter values of T_{air} displayed considerable variation (~–32°C to ~–15°C; Figure 11b). Monthly averaged wind speed and direction (Figures 11c and 11d) also show significant interannual variability. The typical wind direction is approximately toward the south, forcing a net onshore flux of sea ice and the oceanic surface layer along the western ice fronts of WIS.

5. Discussion

[52] From sections 3 and 4, we conclude that changes in the mass balance of WIS in the 2 decades preceding the 2008 and 2009 calving events are driven primarily by a decrease in mean basal melt rate $\langle w_b \rangle$ near 2000, but with a significant contribution from surface processes including SMB and snowmelt (section 3.6 and Figure 5). The surface and basal contributions are out of phase; atmospheric conditions that increase surface accumulation drive an ocean response that reduces basal melt rate. In contrast, a comparison of trends in $h_{i,s}$ (Figure 5c) with the time history of $\langle w_b \rangle$ for GVIIS [*Holland et al.*, 2010, Figure 10] indicates that $\langle w_b \rangle$ increased during the time period 2001–2005 when $dh_{i,s}/dt$ was significantly positive. This result points to distinct, albeit possibly correlated, processes driving the changes in $\langle w_b \rangle$ for WIS and GVIIS.

[53] On the basis of maps of ocean temperature obtained in 2007–2009 by instrumented seals (section 4.1), most of the ice base for the relatively thin WIS is close to the depth of the base of the cold, deep halo of WW surrounding WIS, and well above the core of warm UCDW. Furthermore, recent modeling of WIS and GVIIS basal melt rates by Dinniman et al. (submitted manuscript, 2011) suggests that WIS melting is dominated by seasonal processes whereas GVIIS melting shows smaller seasonal variability (Figure 12) [*Holland et al.*, 2010]. These results lead to the following hypothesis: Excluding intermittent calving events, variations in WIS mass balance are controlled by basal melt rate changes that are sensitive to the depth and circulation of WW rather than the circulation of UCDW. In the remainder of this section, we first compare our basal melt rates with other estimates for WIS and other ice shelves (section 5.1), then expand on our hypothesis with specific consideration for the implications for modeling evolution of thin ice shelves whose bases are sitting in surface-modified water masses (section 5.2).

5.1. Ice-Shelf Mass Loss and Comparisons With Other Ice Shelves

[54] The estimated ice-shelf-averaged basal melt is $\langle w_b \rangle = 1.3 \pm 0.4$ m a^{-1} for the period 1992–2008, and 1.8 ± 0.4 and 0.75 ± 0.55 m a^{-1} for the shorter periods 1992–2000 and 2001–2008, respectively. *Holland et al.* [2010] estimated $\langle w_b \rangle = 0.66$ m a^{-1} for WIS, averaged over the period 1979–2007 (about half of our estimate for roughly the same period). Dinniman et al. (submitted manuscript, 2011) reported a mean value of $\langle w_b \rangle \approx 0.5$ m a^{-1} for the period 2000–2002 (i.e., near the satellite-determined transition in dh_i/dt), but with significant seasonal and interannual variabilities (Figure 12). On the nearby Bach Ice Shelf, *Woodruff and Doake* [1979] estimated a melt rate of 0.65 m a^{-1}.

[55] The rate of net ice volume loss through basal melting for the period 1992–2008, obtained by integrating $\langle w_b \rangle$ over the entire ~13,680 km^2 (pre-2008) area of WIS, was $\sim 18 \pm 6$ km^3 a^{-1}. The net surface accumulation rate was $\sim 9 \pm 4$ km^3 a^{-1}, with a pronounced interannual variability but no significant trend (Figure 5). We estimate that the combined ice volume lost during the calving events in 2008 and 2009 was of the order of 400 km^3, which is equivalent to ~20 years of basal melt at 1992–2008 rates. The preceding large WIS calving event in 1990/1991 resulted in a loss of the order of 100 km^3 [*Braun et al.*, 2009]. Assuming a recurrence interval of ~2 decades for major calving events and a typical loss through the calving of ~250 km^3 (the average of the 1990–1991 and 2008–2009 events), basal melting accounts for about two-thirds of the multidecadal time-averaged mass loss from WIS.

[56] Our estimated value of $\langle w_b \rangle = 1.3 \pm 0.4$ m a^{-1} for WIS for the period 1992–2008 is significantly higher than the mean rates of ~0.1–0.3 m a^{-1} for the large Ross, Filchner-Ronne, and Larsen C ice shelves [*Loose et al.*, 2009; *Joughin and Padman*, 2003; *Holland et al.*, 2009; R. D. Mueller et al., Impact of tide-topography interactions on basal melting of Larsen C Ice Shelf, Antarctica, submitted to *Journal of Geophysical Research*, 2011], and higher than ~0.8 m a^{-1} for Amery Ice Shelf [*Wen et al.*, 2010]. However, it is an order of magnitude lower than ~26 m a^{-1} for Pine Island Glacier (PIG) [*Payne et al.*, 2007]. For GVIIS, the nearest large ice shelf to WIS and sharing a similar oceanographic and geographic setting, *Jenkins and Jacobs* [2008] estimated $\langle w_b \rangle = 3.5$–5 m a^{-1}, based on the hydrographic data from 1994 along the GVIIS southern and northern ice fronts. *Holland et al.* [2010] estimated a mean value of ~2.5 m a^{-1} for GVIIS for the years 1979–2007, although their modeled rates showed significant interannual variability, with annual-averaged $\langle w_b \rangle$ between ~1.5 and ~4 m a^{-1}.

5.2. Environmental Influences on WIS Basal Melt Rate

[57] WIS and GVIIS share comparable topographic settings [*Padman et al.*, 2010; *Graham et al.*, 2011] and have similar satellite-derived trends in dh_i/dt for 1992–2002 [*Zwally et al.*, 2005]. However, in contrast to the *Holland et al.* [2010, Figure 10] estimate of continuous thinning of

GVIIS since 1989, WIS ceased thinning in 2000 (Figure 3), associated with a reduction, at that time, of ~40%–75% in $\langle w_b \rangle$ and an increase in surface accumulation (Figure 5c).

[58] We do not have a continuous series of ocean hydrography surrounding WIS during the transition in $\langle w_b \rangle$ near 2000; however, the record of measured daily sea-ice concentration, which extends back to 1979, shows no evidence for any associated transition in 2000 (Figure 11a). Furthermore, there are no specific shifts near 2000 that can be identified in modeled precipitation (Figure 5) and air temperature and winds (Figures 11b–11d). Nevertheless, we know that there are long-term trends toward warmer, more ice-free conditions on the Bellingshausen Sea continental shelf. *Martinson et al.* [2008] reported long-term changes in hydrographic properties measured during the Palmer LTER program on the continental shelf north of Marguerite Bay, and we hypothesize that the hydrography of the sBS continental shelf surrounding WIS might also be experiencing similar trends. The duration of the summer ice-free period around WIS is increasing (Figure 10b).

[59] How can rapid changes in $\langle w_b \rangle$ arise if trends in environmental forcing have long time scales? The modeled seasonality of $\langle w_b \rangle$ for WIS (Figure 12) and the presence of a cold halo around WIS in T_{180} (Figure 9b) support our hypothesis that WIS $\langle w_b \rangle$ responds primarily to local changes in upper-ocean hydrography and circulation rather than to changes in provision of warm UCDW to the sub-ice-shelf cavity. On the basis of the ocean temperature profile near the ice front (Figure 8b), the mean ice draft ($\langle h_d \rangle$ ~170 m) is close to the depth of the transition from cold WW to the warmer upper thermocline. A relatively small change in depth of the ice base relative to the base of the WW layer can, therefore, significantly change the thermal forcing for melt, (T–T_{freeze}). We estimate that a 10–20 m relative shift in the vertical would change the ocean temperature at the ice base from T ~–1.2°C (upper thermocline) to −1.6°C (WW), compared with the in situ freezing point of $T_{\mathrm{freeze}}(z = 180\ \mathrm{m}) \approx -2.0$°C, roughly halving T–T_{freeze} from 0.8°C to 0.4°C. Assuming a quadratic dependence of w_b [*Holland et al.*, 2008], we expect w_b to decrease by a factor of $\sim(0.4/0.8)^2 = 0.25$. If, instead, we use the empirically derived linear relationship $w_b \propto (T–T_{\mathrm{freeze}})$ proposed by *Rignot and Jacobs* [2002], the ratio of post- to pre- 2000 melt rates is ~0.5. These estimates encompass the ratio of inferred post- and pre-2000 melt rates of ~0.42, taking central estimates of w_b = 0.75 and 1.8 m a^{-1}, respectively (section 3.7). The actual dependence of w_b on T-T_{freeze} probably depends on the causes of ocean velocity under WIS; see the study of Larsen C Ice Shelf by Mueller et al. (submitted manuscript, 2011).

[60] The change in relative location of the ice-shelf base and WW layer base may be driven either by reduction in h_d through ice-shelf thinning or by ocean dynamics. Reduction in h_d over the period 1992–2000 is ~15 m, so that it is plausible that the lower melt rates after 2000 are associated with prior thinning. This model suggests that ice shelves might be able to stabilize once they become sufficiently thin to float in the cold WW layer. However, we cannot easily reconcile this model with an abrupt change in $\langle w_b \rangle$; thus, we also consider the possibility that the transition is driven by changes in the depth of the WW layer in the halo surrounding WIS. Following the study by *Moffat et al.* [2008], we assume that the halo represents a cold, freshwater "coastal" current driven by freshwater inputs (land runoff, sea-ice melt, and ice-shelf basal melting) consolidated by downwelling forced by winds that are usually directed southwards (Figure 11d) [*Hyatt et al.*, 2011]. These competing factors, reduction in melt rate as the ice base rises into cooler water and dependence of melting on the properties of the WW halo, complicate modeling of the response of $\langle w_b \rangle$ to varying environmental conditions such as a trend in large-scale ocean heat transport and changes in sea ice. The latter is a component of the freshwater flux to the upper ocean in summer for subsequent incorporation into the cold halo of WW, and as a potential modifier of momentum transport into the upper ocean to drive circulation and vertical mixing [see *Holland et al.*, 2010].

[61] Modeling basal melt rates is further complicated by the seasonal cycle of ocean heat provision to the sub-ice-shelf cavity. The Dinniman et al. (submitted manuscript, 2011) modeled time series of $\langle w_b \rangle$ for WIS has a pronounced seasonal cycle, with values peaking in March (short-term rates up to 2–6 m a^{-1}) but with essentially no melting between April and November each year (Figure 12). We suspect that this model is inaccurate, as it is based on model geometry (water depth and ice draft) that is now known to be in error. (Modeled channels leading into the WIS cavity are much too shallow compared with recent analyses by *Padman et al.* [2010] and *Graham et al.* [2011], and modeled mean ice draft is only ~120 m, much less than our estimate of ~170 m for 2008). Nevertheless, strong seasonal variability has been observed for other ice shelves including the following: PIG ice shelf, where w_b near the grounding line varies quasi-annually by $O(100)$ m a^{-1} [*Bindschadler et al.*, 2011] and Ronne Ice Shelf, which shows strong seasonality in the temperature and volume flux of inflowing high salinity shelf water [*Nicholls*, 1996; *Nicholls and Makinson*, 1998]. Note that neither the *Holland et al.* [2010] nor the Dinniman et al. (submitted manuscript, 2011) models show significant seasonality in $\langle w_b \rangle$ for GVIIS (see also Figure 12).

[62] Some of the seasonal change in ventilation of ice shelves can be attributed to annual cycles of the large-scale wind stress; for example, the quasi-annual cycle in ventilation of the PIG ice shelf cavity has been attributed to seasonal forcing of warm CDW through the trough leading from the continental shelf break into Pine Island Bay [*Thoma et al.*, 2008]. However, measurements made along the Ronne Ice Shelf front led *Makinson et al.* [2006] to conclude that seasonality in ventilation of the sub-ice-shelf cavity was driven, at least in part, by changes in stratification just seaward of the ice front. When the water column is unstratified, water is forced to flow parallel to a uniform-thickness ice front by conservation of potential vorticity. However, this constraint is weakened when stratification is established in summer by insolation and ice melt. Other factors, including wind stress and sea ice, also vary significantly on a seasonal cycle.

[63] As with the cold WW halo around WIS, dependence of annual mean basal melt on seasonally varying environmental conditions implies that numerical models for predicting w_b must be capable of accurately resolving fairly small-scale processes acting on short time scales. These processes include complex interactions between coastal wind stress, surface radiation balance, sea ice, and freshwater

fluxes (including land runoff, sea-ice production and melt, and feedbacks between the ice shelf and regional hydrography and circulation).

[64] The preceding discussion ignores spatial variability of w_b; however, based on local mass balance estimates, the pre-2000 values of dh_i/dt at specific crossovers (Figure 2) range from approximately in balance with SMB and divergence in the north, to $\sim$0.31 m a^{-1} near the eastern end of Latady Island (X_{313}) and $-$0.43 m a^{-1} near the glacier inlet at X_{306}. At X_{313}, which is close to the site of the first calving event in 2008, thinning continued through 2008 (Figure 3), with total estimated thinning of $\sim$80 m from 1978 to 2008 [*Fricker and Padman*, 2012]. Thinning of this magnitude and spatial variability may be sufficient to precondition the ice shelf for rapid calving and retreat as stresses change within the ice-shelf plate [*Khazendar et al.*, 2007; *Vieli et al.*, 2007; *Glasser and Scambos*, 2008].

6. Conclusions

[65] WIS thinned prior to 2000, consistent with an ice-shelf-averaged basal melt rate of $w_b = 1.8 \pm 0.4$ m a^{-1} that exceeds the equilibrium value of 0.5 ± 0.3 m a^{-1} required to balance surface mass accumulation ($\sim 0.7 \pm 0.3$ m a^{-1}, ice-equivalent thickness) plus the ice-shelf-averaged ice divergence ($\sim$–0.2 m a^{-1}). Between 2000 and the major calving events of 2008 and 2009, thinning for most of WIS was negligible. It is intriguing that most of WIS stopped thinning $\sim$8 years before the first major calving events in 2008. (This is in contrast to Larsen B Ice Shelf, which experienced surface lowering at $\sim$0.2 m a^{-1} up to the time of its collapse in 2002 [*Fricker and Padman*, 2012].) Steady-state ice thickness is, therefore, not a sufficient condition for identifying ice-shelf stability.

[66] The 3-D distribution of ocean temperature T indicates strong lateral variability at the approximate mean depth of the WIS base (Figure 9b). We attribute the deepening of upper-ocean layers around WIS to coastal (ice front) downwelling associated with the generally southward wind stress (Figure 11), possibly augmented by freshwater fluxes from the AP, melting sea ice, and basal melting of WIS and GVIIS [see also *Moffat et al.*, 2008].

[67] We found no evidence for a rapid change in environmental conditions (measured sea-ice concentration and modeled atmospheric variables) to explain the transition in w_b near 2000. Instead, we hypothesize that this transition represents a change in the relative position of the ice base and the base of the cold WW layer sitting on top of the warmer water of the main thermocline (Figure 8b). We lack the data to determine whether this relative elevation change arises from thinning of the ice shelf or a depression of the WW layer in the cold halo around WIS (Figure 9b). However, we emphasize that the presence of regions of high dT/dz in the ocean can enhance variability in w_b in response to small perturbations in processes contributing to ice-shelf thickness changes and upper-ocean hydrography.

[68] The hypothesized sensitivity of w_b to ice draft relative to the depth of the WW layer, and the lateral variability of upper-ocean temperature, indicate that w_b depends on the details of ocean response to processes occurring fairly close to WIS. We expect that ocean models forced by coarse-grid atmospheric models that fail to resolve wind stress variability induced by coastal topography will be unable to accurately represent the water masses advected into the sub-ice-shelf cavity near the depth of the ice base. Furthermore, if the observed depression of isotherms around WIS is influenced by freshwater fluxes from the AP coast and ice-shelf bases, an accurate climate model must also adequately represent these fluxes. *Moffat et al.* [2008] noted that the spatial distribution of freshwater flux to the Bellingshausen Sea in summer is sensitive to the representation of orography in atmospheric models. The steep, narrow mountain range of the AP will be insufficiently resolved even in the relatively high-resolution (δx = 14 km) RACMO model discussed by *Moffat et al.* [2008], leading to potentially large errors in the magnitude and distribution of freshwater sources.

[69] Our result, that WIS melting is strongly influenced by small-scale coastal atmospheric and oceanic processes, is in contrast to ice shelves influenced primarily by the strength and temperature of deep CDW inflows along troughs. For the latter type of ice shelf (e.g., PIG and Thwaites ice shelves in Pine Island Bay and GVIIS), the larger-scale wind forcing is more important as the driver of CDW upwelling at the continental shelf break and subsequent intrusions through troughs to the ice-shelf cavities.

[70] In summary, changes in WIS basal melt are determined primarily by coastal atmospheric and oceanic processes that assist ventilation of the sub-ice-shelf cavity by upper-ocean water masses, rather than by the more frequently reported mechanism of large-scale atmospheric forcing of benthic inflows of warm CDW along troughs cutting across the continental shelf [e.g., *Thoma et al.*, 2008]. The implied sensitivity of basal melt rate to processes acting on short spatial scales (e.g., downwelling and coastal currents enhanced by freshwater fluxes from runoff and ice-shelf basal melt) and with strong seasonal dependence implies that existing oceanographic observations, which are sparse and strongly biased toward summer sampling because of logistic constraints imposed by sea ice, will not adequately represent the annual averages of ice-shelf mass loss through melting. We conclude that progress in understanding basal melting, particularly of relatively thin ice shelves whose bases sit in upper-ocean water masses modified by local ocean/atmosphere interactions, requires development of high-resolution models of both the atmosphere and ocean with accurate geometry (mountain and glacier topography, ice draft, and seabed bathymetry). We also require long-term simultaneous measurements of all major components of the Antarctic coastal climate system, for validating climate system models and identifying processes that are presently unrepresented in models.

Appendix A: Acquisition and Processing of CTD Data From Instrumented Seals

[71] Hydrographic data used in this study were obtained from a total of 38 southern elephant seals (*Mirounga leonina*) that were instrumented in 2007 (12 seals), 2008 (12 seals) and 2009 (14 seals) after molting at the Cape Shirreff rookery on Livingston Island in the South Shetland Islands, Antarctica. Each seal was equipped with a CTD-SRDL (or "tag") manufactured by the Sea Mammal

Research Unit of St. Andrews, UK, incorporating a CTD sensor built by Valeport Ltd., Totnes, UK.

[72] Before deployment, the CTD-SRDLs were calibrated at the Naval Postgraduate School (Monterey, California), with resolutions for T and C of 0.001°C and 0.002 mS cm^{-1}, respectively [*Boehme et al.*, 2009]. The tags fall off when the seal molts, occasionally earlier; thus, no postcalibrations are possible to assess potential changes in accuracy during the operational lifetime of tags used for the present study. However, three CTD-SRDL tags that were deployed on northern elephant seals and recovered after 72–136 day deployments showed no change in calibration within the manufacturer's specifications.

[73] The data acquired during each dive was transmitted through the Argos satellite system each time a seal surfaced. Position data from Argos were processed as described in the study by *Padman et al.* [2010]: Typical lateral displacement for each dive was less than 0.5 km, and the 99% confidence level for true position for each individual dive location was within ~4 km of the reported position.

[74] Hydrographic profiles were obtained by measuring C, T, and D (derived from pressure P) every 4 s during the ascent phase of each seal dive. Salinity (S) was derived from P, T, and C through standard algorithms. Because of the narrow bandwidth of Argos transmitters, data were preprocessed by the CTD-SRDL sensor before being transmitted via the Argos system. Each profile of 4 s data was compressed to a set of 12 data points corresponding to the most important inflection points determined with a "broken stick" algorithm [*Boehme et al.*, 2009]. Maximum dive depth (D_{max}) was also recorded for each dive. Each seal tag provided ~2–5 hydrographic profiles per day, with an average value for all tags of 3.0 profiles per day. On the basis of the comparisons of D_{max} with ship-based bathymetry data, about 30% of all seal dives over the Bellingshausen Sea continental shelf reached the seabed [*Padman et al.*, 2010], consistent with the known foraging behavior of elephant seals [*McConnell et al.*, 1992; *Costa et al.*, 2010].

[75] **Acknowledgments.** ERS and Envisat radar altimeter data is copyright to ESA and was provided by Jay Zwally at the Cryospheric Sciences Branch of the Hydrospheric and Biospheric Sciences Laboratory of NASA/GSFC, with special thanks to Jairo Santana and Helen Cornejo (http://icesat4.gsfc.nasa.gov/). We thank David Sandwell for providing the high-resolution bathymetry grids; Patrick Robinson for calibration and preparation of, and Birgitte McDonald for deployment of, the seal CTD tags. This study was supported by NASA grants NNG05GR58G, NNX06AD40G, and NNG06GA69G to L.P., H.A.F, and T.A.S., respectively; ONR grant N00014-05-1-0645 to D.P.C.; and NSF grants OPP-0338101 to ESR, ANT-0440687 and ANT-0523332 to D.P.C., and ANT-0523172 to ODU. We acknowledge support from Utrecht University and the Netherlands Polar Program of the Netherlands Organization of Scientific Research (NWO/ALW). This is ESR contribution 146.

References

Arthern, R. J., D. P. Winebrenner, and D. G. Vaughan (2006), Antarctic snow accumulation mapped using polarization of 4.3-cm wavelength microwave emission, *J. Geophys. Res.*, *111*, D06107, doi:10.1029/2004JD005667.

Bamber, J. L., and R. A. Bindschadler (1997), An improved elevation data set for climate and ice sheet modelling: Validation with satellite imagery, *Ann. Glaciol.*, *25*, 439–444.

Bamber, J. L., J. L. Gomez-Dans, and J. A. Griggs (2009), A new 1 km digital elevation model of the Antarctic derived from combined satellite radar and laser data–Part 1: Data and methods, *Cryosphere*, *3*, 101–111, doi:10.5194/tc-3-101-2009.

Bindschadler, R., D. G. Vaughan, and P. Vornberger (2011), Variability of basal melt beneath the Pine Island Glacier Ice Shelf, West Antarctica, *J. Glaciol.*, *57*, 581–595, doi:10.3189/002214311797409802.

Biuw, M., et al. (2007), Variations in behavior and condition of a Southern Ocean top predator in relation to in situ oceanographic conditions, *Proc. Natl. Acad. Sci. U. S. A.*, *104*, 13,705–13,710, doi:10.1073/pnas.0701121104.

Boehme, L., P. Lovell, M. Biuw, F. Roquet, J. Nicholson, S. E. Thorpe, M. P. Meredith, and M. Fedak (2009), Technical note: Animal-borne CTD-Satellite Relay Data Loggers for real-time oceanographic data collection, *Ocean Sci.*, *5*, 685–695, doi:10.5194/os-5-685-2009.

Braun, M., and A. Humbert (2009), Recent retreat of Wilkins Ice Shelf reveals new insights in ice shelf break-up mechanisms, *Geosci. Remote Sens. Lett.*, *6*, 263–267, doi:10.1109/LGRS.2008.2011925.

Braun, M., A. Humbert, and A. Moll (2009), Changes of Wilkins Ice Shelf over the past 15 years and inferences on its stability, *Cryosphere*, *3*, 41–56, doi:10.5194/tc-3-41-2009.

Bromirski, P. D., O. V. Sergienko, and D. R. MacAyeal (2010), Transoceanic infragravity waves impacting Antarctic ice shelves, *Geophys. Res. Lett.*, *37*, L02502, doi:10.1029/2009GL041488.

Brooks, R. L., R. S. Williams Jr., J. G. Ferrigno, and W. B. Krabill (1983), Amery ice shelf topography from satellite radar altimetry, in *Antarctic Earth Science*, edited by R. L. Oliver et al., pp. 441–445, Aust. Acad. Sci., Canberra, Australia, and Cambridge Univ. Press, Cambridge, U. K.

Burns, J. M., D. P. Costa, M. A. Fedak, M. A. Hindell, C. J. A. Bradshaw, N. J. Gales, B. McDonald, S. J. Trumble, and D. E. Crocker (2004), Winter habitat use and foraging behavior of crabeater seals along the Western Antarctic Peninsula, *Deep Sea Res., Part II*, *51*, 2279–2303, doi:10.1016/j.dsr2.2004.07.021.

Cavalieri, D. J., and C. L. Parkinson (2008), Antarctic sea ice variability and trends, 1979–2006, *J. Geophys. Res.*, *113*, C07004, doi:10.1029/2007JC004564.

Cavalieri, D. J., P. Gloersen, and W. J. Campbell (1984), Determination of sea ice parameters with Nimbus 7 SMMR, *J. Geophys. Res.*, *89*, 5355–5369, doi:10.1029/JD089iD04p05355.

Cavalieri, D. J., C. Parkinson, P. Gloersen, and H. J. Zwally (1996), *Sea ice concentrations from Nimbus-7 SMMR and DMSP SSM/I passive microwave data, 1978–2008, digital media, updated 2006*, Natl. Snow and Ice Data Cent., Boulder, Colo.

Charrassin, J.-B., et al. (2008), Southern Ocean frontal structure and sea-ice formation rates revealed by elephant seals, *Proc. Natl. Acad. Sci. U. S. A.*, *105*, 11,634–11,639, doi:10.1073/pnas.0800790105.

Cook, A. J., and D. G. Vaughan (2010), Overview of areal changes of the ice shelves on the Antarctic Peninsula over the past 50 years, *Cryosphere*, *4*, 77–98, doi:10.5194/tc-4-77-2010.

Cook, A. J., A. J. Fox, D. G. Vaughan, and J. G. Ferrigno (2005), Retreating glacier fronts on the Antarctic Peninsula over the past half-century, *Science*, *308*, 541–544, doi:10.1126/science.1104235.

Costa, D. P., J. M. Klinck, E. E. Hofmann, M. S. Dinniman, and J. M. Burns (2008), Upper ocean variability in west Antarctic Peninsula continental shelf waters as measured using instrumented seals, *Deep Sea Res., Part II*, *55*, 323–337, doi:10.1016/j.dsr2.2007.11.003.

Costa, D. P., L. A. Huckstadt, D. E. Crocker, B. I. McDonald, M. E. Goebel, and M. A. Fedak (2010), Approaches to studying climatic change and its role on the habitat selection of Antarctic pinnipeds, *Integr. Comp. Biol.*, *50*, 1018–1030, doi:10.1093/icb/icq054.

Cox, L. H., and R. S. March (2004), Comparison of geodetic and glaciological mass balance techniques, Gulkana Glacier, Alaska, U.S.A, *J. Glaciol.*, *50*, 363–370, doi:10.3189/172756504781829855.

Dee, D. P., et al. (2011), The ERA-Interim reanalysis: Configuration and performance of the data assimilation system, *Q. J. R. Meteorol. Soc.*, *137*, 553–597, doi:10.1002/qj.828.

Dinniman, M. S., and J. M. Klinck (2004), A model study of circulation and cross shelf exchange on the west Antarctic Peninsula continental shelf, *Deep Sea Res., Part II*, *51*, 2003–2022, doi:10.1016/j.dsr2.2004.07.030.

Dorland, R. D., and M. Zhou (2008), Circulation and heat fluxes during the austral fall in George VI Sound, Antarctic Peninsula, *Deep Sea Res., Part II*, *55*, 294–308, doi:10.1016/j.dsr2.2007.01.014.

Fricker, H. A., and L. Padman (2006), Ice shelf grounding zone structure from ICESat laser altimetry, *Geophys. Res. Lett.*, *33*, L15502, doi:10.1029/2006GL026907.

Fricker, H. A., and L. Padman (2012), Thirty years of elevation change on Antarctic Peninsula ice shelves from multi-mission satellite radar altimetry, *J. Geophys. Res.*, doi:10.1029/2011JC007126, in press.

Fricker, H. A., G. Hyland, R. Coleman, and N. W. Young (2000), Digital elevation models for the Lambert Glacier-Amery Ice Shelf system, East Antarctica, from ERS-1 satellite radar altimetry, *J. Glaciol.*, *46*, 553–560, doi:10.3189/172756500781832639.

Fricker, H. A., S. Popov, I. Allison, and N. Young (2001), Distribution of marine ice beneath the Amery Ice Shelf, *Geophys. Res. Lett.*, *28*, 2241–2244, doi:10.1029/2000GL012461.

Fricker, H. A., N. W. Young, I. Allison, and R. A. Coleman (2002), Iceberg calving from the Amery Ice Shelf, East Antarctica, *Ann. Glaciol.*, *34*, 241–246, doi:10.3189/172756402781817581.

Glasser, N. F., and T. A. Scambos (2008), A structural glaciological analysis of the 2002 Larsen B Ice Shelf collapse, *J. Glaciol.*, *54*, 3–16, doi:10.3189/002214308784409017.

Graham, A. G. C., F. O. Nitsche, and R. D. Larter (2011), An improved bathymetry compilation for the Bellingshausen Sea, Antarctica, to inform ice-sheet and ocean models, *Cryosphere*, *5*, 95–106, doi:10.5194/tc-5-95-2011.

Gray, A. L., K. E. Matter, and G. Sofko (2000), Influence of ionospheric electron density fluctuations on satellite radar interferometry, *Geophys. Res. Lett.*, *27*, 1451–1454, doi:10.1029/2000GL000016.

Griggs, J. A., and J. L. Bamber (2009), A new 1 km digital elevation model of Antarctica derived from combined radar and laser data–Part 2: Validation and error estimates, *Cryosphere*, *3*, 113–123, doi:10.5194/tc-3-113-2009.

Helsen, M. M., M. R. van den Broeke, R. S. W. van de Wal, W. J. van de Berg, E. van Meijgaard, C. H. Davis, Y. Li, and I. Goodwin (2008), Elevation changes in Antarctica mainly determined by accumulation variability, *Science*, *320*, 1626–1629, doi:10.1126/science.1153894.

Holland, P. R., A. Jenkins, and D. M. Holland (2008), The response of ice shelf basal melting to variations in ocean temperature, *J. Clim.*, *21*, 2558–2572, doi:10.1175/2007JCLI1909.1.

Holland, P. R., H. F. J. Corr, D. G. Vaughan, A. Jenkins, and P. Skvarca (2009), Marine ice in Larsen Ice Shelf, *Geophys. Res. Lett.*, *36*, L11604, doi:10.1029/2009GL038162.

Holland, P. R., A. Jenkins, and D. M. Holland (2010), A regional model of ocean processes in the Bellingshausen Sea, Antarctica, *J. Geophys. Res.*, *115*, C05020, doi:10.1029/2008JC005219.

Howard, S. L., J. Hyatt, and L. Padman (2004), Mixing in the pycnocline over the western Antarctic Peninsula Shelf during Southern Ocean GLOBEC, *Deep Sea Res., Part II*, *51*, 1965–1979, doi:10.1016/j.dsr2.2004.08.002.

Humbert, A., and M. Braun (2008), The Wilkins Ice Shelf, Antarctica: Break-up along failure zones, *J. Glaciol.*, *54*, 943–944, doi:10.3189/002214308787780012.

Humbert, A., D. Gross, R. Müller, M. Braun, R. S. W. van de Wal, M. R. van den Broeke, D. G. Vaughan, and W. J. van de Berg (2010), Deformation and failure of the ice bridge on Wilkins Ice Shelf, Antarctica, *Ann. Glaciol.*, *51*, 49–55, doi:10.3189/172756410791392709.

Hyatt, J., R. C. Beardsley, and W. B. Owens (2011), Characterization of sea ice cover, motion and dynamics in Marguerite Bay, Antarctic Peninsula, *Deep Sea Res., Part II*, *58*, 1553–1568, doi:10.1016/j.dsr2.2010.08.021.

Jacobs, S. S., and J. C. Comiso (1997), Climate variability in the Amundsen and Bellingshausen seas, *J. Clim.*, *10*, 697–709, doi:10.1175/1520-0442(1997)010<0697:CVITAA>2.0.CO;2.

Jenkins, A., and S. S. Jacobs (2008), Circulation and melting beneath George VI Ice Shelf, Antarctica, *J. Geophys. Res.*, *113*, C04013, doi:10.1029/2007JC004449.

Joughin, I. (2002), Ice-sheet velocity mapping: A combined interferometric and speckle-tracking approach, *Ann. Glaciol.*, *34*, 195–201, doi:10.3189/172756402781817978.

Joughin, I., and L. Padman (2003), Melting and freezing beneath Filchner-Ronne Ice Shelf, Antarctica, *Geophys. Res. Lett.*, *30*(9), 1477, doi:10.1029/2003GL016941.

Khazendar, A., E. Rignot, and E. Larour (2007), Larsen B Ice Shelf rheology preceding its disintegration inferred by a control method, *Geophys. Res. Lett.*, *34*, L19503, doi:10.1029/2007GL030980.

Klinck, J. M., E. E. Hofmann, R. C. Beardsley, B. Salihoglu, and S. L. Howard (2004), Water-mass properties and circulation on the west Antarctic Peninsula continental shelf in austral fall and winter 2001, *Deep Sea Res., Part II*, *51*, 1925–1946, doi:10.1016/j.dsr2.2004.08.001.

Lachlan-Cope, T., and W. Connolley (2006), Teleconnections between the tropical Pacific and the Amundsen-Bellinghausens Sea: Role of the El Niño/Southern Oscillation, *J. Geophys. Res.*, *111*, D23101, doi:10.1029/2005JD006386.

Lazzara, M. A., K. C. Jezek, T. A. Scambos, D. R. MacAyeal, and C. J. van der Veen (1999), On the Recent Calving of Icebergs from the Ross Ice Shelf, *Polar Geogr.*, *23*, 201–212, doi:10.1080/10889379909377676.

Ligtenberg, S. R. M., M. M. Helsen, and M. R. van den Broeke (2011), An improved semi-empirical model for the densification of Antarctic firn, *Cryosphere*, *5*, 809–819, doi:10.5194/tc-5-809-2011.

Loose, B., P. Schlosser, W. M. Smethie, and S. S. Jacobs (2009), An optimized estimate of glacial melt from the Ross Ice Shelf using noble gases, stable isotopes, and CFC transient tracers, *J. Geophys. Res.*, *114*, C08007, doi:10.1029/2008JC005048.

Lucchitta, B., and C. Rosanova (1998), Retreat of northern margins of George VI and Wilkins ice shelves, Antarctic Peninsula, *Ann. Glaciol.*, *27*, 41–46.

MacAyeal, D. R., T. A. Scambos, C. Hulbe, and M. A. Fahnestock (2003), Catastrophic ice-shelf break-up by an ice-shelf-fragment-capsize mechanism, *J. Glaciol.*, *49*, 22–36, doi:10.3189/172756503781830863.

MacAyeal, D. R., J. N. Bassis, E. A. Okal, R. C. Aster, and L. M. Cathles (2008), Ocean wave generation by collapsing ice shelves, *Eos Trans. AGU*, *89*(53), Fall Meet. Suppl., Abstract C41D–08.

Makinson, K., M. Schröder, and S. Østerhus (2006), Effect of critical latitude and seasonal stratification on tidal current profiles along Ronne Ice Front, Antarctica, *J. Geophys. Res.*, *111*, C03022, doi:10.1029/2005JC003062.

Martinson, D. G., S. E. Stammerjohn, R. A. Iannuzzi, R. C. Smith, and M. Vernet (2008), Western Antarctic Peninsula physical oceanography and spatio-temporal variability, *Deep Sea Res., Part II*, *55*, 1964–1987, doi:10.1016/j.dsr2.2008.04.038.

Massom, R. A., S. E. Stammerjohn, W. Lefebvre, S. A. Harangozo, N. Adams, T. A. Scambos, M. J. Pook, and C. Fowler (2008), West Antarctic Peninsula sea ice in 2005: Extreme ice compaction and ice edge retreat due to strong anomaly with respect to climate, *J. Geophys. Res.*, *113*, C02S20, doi:10.1029/2007JC004239.

McConnell, B. J., C. Chambers, and M. A. Fedak (1992), Foraging ecology of southern elephant seals in relation to the bathymetry and productivity of the Southern Ocean, *Antarct. Sci.*, *4*, 393–398, doi:10.1017/S0954102092000580.

Moffat, C., R. C. Beardsley, B. Owens, and N. van Lipzig (2008), A first description of the Antarctic Peninsula Coastal Current, *Deep Sea Res., Part II*, *55*, 277–293, doi:10.1016/j.dsr2.2007.10.003.

Nicholls, K. W. (1996), Temperature variability beneath Ronne Ice Shelf, Antarctica, from thermistor cables, *J. Geophys. Res.*, *101*, 1199–1210, doi:10.1029/95JC02679.

Nicholls, K. W., and K. Makinson (1998), Ocean circulation beneath the western Ronne Ice Shelf, as derived from in situ measurements of water currents and properties, in *Ocean, Ice, and Atmosphere: Interactions at the Antarctic Continental Margin*, edited by S. S. Jacobs and R. F. Weiss, pp. 301–318, AGU, Washington, D. C., doi:10.1029/AR075p0301.

Nicholls, K. W., L. Boehme, M. Biuw, and M. A. Fedak (2008), Wintertime ocean conditions over the southern Weddell Sea continental shelf, Antarctica, *Geophys. Res. Lett.*, *35*, L21605, doi:10.1029/2008GL035742.

Padman, L., D. P. Costa, S. T. Bolmer, M. E. Goebel, L. A. Huckstadt, A. Jenkins, B. I. McDonald, and D. R. Shoosmith (2010), Seals map bathymetry of the Antarctic continental shelf, *Geophys. Res. Lett.*, *37*, L21601, doi:10.1029/2010GL044921.

Pavlis, N. K., S. A. Holmes, S. C. Kenyon, and J. K. Factor (2008), An Earth gravitational model to degree 2160: EGM2008, paper presented at the General Assembly of the European Geosciences Union, Vienna, Austria, 13–18 April.

Payne, A. J., P. R. Holland, A. P. Shepherd, I. C. Rutt, A. Jenkins, and I. Joughin (2007), Numerical modeling of ocean/ice interactions under Pine Island Bay's ice shelf, *J. Geophys. Res.*, *112*, C10019, doi:10.1029/2006JC003733.

Rignot, E., and S. S. Jacobs (2002), Rapid bottom melting widespread near Antarctic ice sheet grounding lines, *Science*, *296*, 2020–2023, doi:10.1126/science.1070942.

Robertson, R. A., M. Visbeck, A. L. Gordon, and E. Fahrbach (2002), Long-term temperature trends in the deep waters of the Weddell Sea, *Deep Sea Res., Part II*, *49*, 4791–4806, doi:10.1016/S0967-0645(02)00159-5.

Scambos, T. A., C. Hulbe, and M. Fahnestock (2003), Climate-induced ice shelf disintegration in the Antarctic Peninsula, in *Antarctic Peninsula Climate Variability; Historical and Paleoenvironmental Perspectives*, edited by E. Domack et al., pp. 79–92, AGU, Washington, D. C., doi:10.1029/AR079p0079.

Scambos, T. A., M. A. Fahnestock, T. Haran, and J. Bohlander (2007), A MODIS-based Mosaic of Antarctica: MOA, *Remote Sens. Environ.*, *111*, 242–257, doi:10.1016/j.rse.2006.12.020.

Scambos, T. A., H. A. Fricker, C.-C. Liu, J. Bohlander, J. Fastook, A. Sargent, R. Massom, and A.-M. Wu (2009), Ice shelf disintegration by plate bending and hydrofracture: Satellite observations and model results of the 2008 Wilkins Ice Shelf break-up, *Earth Planet. Sci. Lett.*, *280*, 51–60, doi:10.1016/j.epsl.2008.12.027.

Shepherd, A., D. Wingham, T. Payne, and P. Skvarca (2003), Larsen Ice Shelf has progressively thinned, *Science*, *302*, 856–859, doi:10.1126/science.1089768.

Shepherd, A., D. Wingham, T. Payne, and P. Skvarca (2004), Correction to "Larsen Ice Shelf has progressively thinned," *Science*, *303*, 1612.

Stammerjohn, S. E., D. G. Martinson, R. C. Smith, and R. A. Iannuzzi (2008), Sea ice in the western Antarctic Peninsula region: Spatio-temporal variability from ecological and climate change perspectives, *Deep Sea Res., Part II*, *55*, 2041–2058, doi:10.1016/j.dsr2.2008.04.026.

Thoma, M., A. Jenkins, D. M. Holland, and S. S. Jacobs (2008), Modelling Circumpolar Deep Water intrusions on the Amundsen Sea continental shelf, Antarctica, *Geophys. Res. Lett.*, *35*, L18602, doi:10.1029/2008GL034939.

van de Berg, W. J., M. R. van den Broeke, and E. van Meijgaard (2006), Reassessment of the Antarctic surface mass balance using calibrated output of a regional atmospheric climate model, *J. Geophys. Res.*, *111*, D11104, doi:10.1029/2005JD006495.

van den Broeke, M. R. (2005), Strong surface melting preceded collapse of Antarctic Peninsula ice shelf, *Geophys. Res. Lett.*, *32*, L12815, doi:10.1029/2005GL023247.

Vaughan, D. G., and C. S. M. Doake (1996), Recent atmospheric warming and retreat of ice shelves on the Antarctic Peninsula, *Nature*, *379*, 328–331, doi:10.1038/379328a0.

Vaughan, D. G., D. R. Mantripp, J. Sievers, and C. S. M. Doake (1993), A synthesis of remote sensing data on Wilkins Ice Shelf, Antarctica, *Ann. Glaciol.*, *17*, 211–218.

Vieli, A., A. J. Payne, A. Shepherd, and Z. Du (2007), Causes of pre-collapse changes of the Larsen B ice shelf: Numerical modeling and assimilation of satellite observations, *Earth Planet. Sci. Lett.*, *259*, 297–306, doi:10.1016/j.epsl.2007.04.050.

Walker, D. P., M. A. Brandon, A. Jenkins, J. T. Allen, J. A. Dowdeswell, and J. Evans (2007), Oceanic heat transport onto the Amundsen Sea shelf through a submarine glacial trough, *Geophys. Res. Lett.*, *34*, L02602, doi:10.1029/2006GL028154.

Wen, J., Y. Wang, W. Wang, K. C. Jezek, H. Liu, and I. Allison (2010), Basal melting and freezing under the Amery Ice Shelf, East Antarctica, *J. Glaciol.*, *56*, 81–90, doi:10.3189/002214310791190820.

Williams, G. D., M. Hindell, M.-N. Houssais, T. Tamura, and I. C. Field (2011), Upper ocean stratification and sea ice growth rates during the summer-fall transition, as revealed by Elephant seal foraging in the Adélie Depression, East Antarctica, *Ocean Sci.*, *7*, 185–202, doi:10.5194/os-7-185-2011.

Woodruff, A. H. W., and C. S. M. Doake (1979), Depolarization of radio waves can distinguish between floating and grounded ice sheets, *J. Glaciol.*, *23*, 223–232.

Yi, D., H. J. Zwally, and J. W. Robbins (2011), ICESat observations of seasonal and interannual variations of sea-ice freeboard and estimated thickness in the Weddell Sea, Antarctica (2003–2009), *Ann. Glaciol.*, *52*, 43–51, doi:10.3189/172756411795931480.

Zwally, H. J., R. A. Bindschadler, A. C. Brenner, J. A. Major, and J. G. Marsh (1989), Growth of Greenland Ice Sheet: Measurement, *Science*, *246*, 1587–1589, doi:10.1126/science.246.4937.1587.

Zwally, H. J., M. B. Giovinetto, J. Li, H. G. Cornejo, M. A. Beckley, A. C. Brenner, J. L. Saba, and D. Yi (2005), Mass changes of the Greenland and Antarctic ice sheets and shelves and contributions to sea-level rise: 1992–2002, *J. Glaciol.*, *51*, 509–527, doi:10.3189/172756505781829007.

D. P. Costa, Ecology and Evolutionary Biology, University of California, Santa Cruz, CA 95060, USA.

M. S. Dinniman, Center for Coastal Physical Oceanography, Old Dominion University, Norfolk, VA 23508, USA.

H. A. Fricker, Institute of Geophysics and Planetary Physics, Scripps Institution of Oceanography, University of California, San Diego, La Jolla, CA 92037, USA.

M. E. Goebel, Antarctic Ecosystem Research Division, SWFSC, National Marine Fisheries Service, NOAA, La Jolla, CA 92037-1508, USA.

L. A. Huckstadt, Ocean Sciences, University of California, Santa Cruz, CA 95060, USA.

A. Humbert, Institute of Geophysics, University of Hamburg, KlimaCampus, D-20146 Hamburg, Germany.

I. Joughin, Polar Science Center, Applied Physics Laboratory, University of Washington, Seattle, WA 98105-6698, USA.

J. T. M. Lenaerts, S. R. M. Ligtenberg, and M. R. van den Broeke, Institute for Marine and Atmospheric Research Utrecht, Utrecht University, NL-3584 CC Utrecht, Netherlands.

L. Padman, Earth and Space Research, Corvallis, OR 97333-1536, USA. (padman@esr.org)

T. Scambos, National Snow and Ice Data Center, CIRES, University of Colorado at Boulder, Boulder, CO 80309-0449, USA.